Integrated Thermomechanical Model of First Wall Components Under Evolving Chemistry and Microstructure During Fusion Reactor Operation (ThermChem-FW)

Applicant:
The Regents of the University of California, Los Angeles
10889 Wilshire Boulevard
Los Angeles, CA 90095-1406

Lead PI:
Jaime Marian
Phone: (310) 206-9161*, email:* jmarian@ucla.edu

Administrative Point of Contact:
Rachel Tat
UCLA's Office of Contracts and Grants
Phone: (310) 983-3529*, email:* rachel.tat@research.ucla.edu

Funding Opportunity FOA Number: DE-FOA-0002924
DOE/Office of Science Program Office: Fusion Energy Sciences
DOE/Office of Science Program Office Technical Contact: Michael Halfmoon

PAMS Pre-proposal tracking number: PRE-0000034902
Research area identified in Section I of this FOA: First Wall and Beyond

Supplement to cover page for details on collaboration

Collaborating Institutions:

University of California Los Angeles	Jaime Marian
Stony Brook University	Jason Trelewicz
University of Wisconsin	Izabela Szlufarska
University of Miami	Giacomo Po
Villanova University	David Cereceda
Sandia National Laboratories	Mary Alice Cusentino, Khachik Sargsyan
Pacific Northwest National Laboratory	Wahyu Setyawan
Oak Ridge National Laboratory	David Bernholdt, Paul Humrickhouse
Idaho National Laboratory	Cody Permann, Benjamin Spencer

Lead PI: Jaime Marian

Leadership structure of the collaboration: This project is structured as a Center (which will be referred to as 'ThermChem-FW' Center) an assembly of three spatiotemporal levels, each capturing different length and timescales for the purpose of developing an integrated computational model to predict first wall/blanket performance. Each level will have a designated coordinator to manage level-specific research tasks and facilitate communication between levels. *Marian* (UCLA) will act as executive project director, supervising and coordinating all research activities by interacting directly with level coordinators. *Trelewicz* (Stony Brook) will serve as deputy director and coordinator for Level 1 (materials properties at the atomic scale), which in addition includes *Szlufarska* (Wisconsin), *Cereceda* (Villanova), *Cusentino* and *Sargsyan* (SNL), and *Setyawan* (PNNL). Level 2 (microstructural evolution) will be coordinated by *Marian* (UCLA) and includes *Po* (Miami) and *Humrickhosue* (ORNL). Finally, Level 3 (device thermomechanical response simulations) will be coordinated by *Permann* (INL) and also includes *Spencer* (INL) and *Bernholdt* (ORNL). Specific project members will also be designated to act as liaisons between the different levels, ensuring information flow and useful feedback in both directions. The project is thus built around teams that blend materials scientists with applied mathematicians, merging their expertises to maximize synergisms and provide joint solutions to each technical challenge.

Description of each collaborating institution's facilities, equipment, and resources: All participating institutions will utilize a flexible computing approach, combining software development and testing on local institutional computational resources with large-scale runs on DOE leadership-class architectures through the INCITE program. Details about these computational facilities are provided in Appendix 2 of this proposal.

Training and mentoring of students and junior researchers by the collaborators: We will make student training and workforce development in fusion energy materials and in theory, modeling and simulation one of the top priorities in this project. Among all the participating institutions, this proposal calls for the involvement of a total of 8 graduate students and 7 postdoctoral researchers at any given time in the various project activities. The work of all junior personnel (students and postdocs) will be guided and monitored by the proposal co-PIs on a weekly basis. The duration of a postdoctoral term at most institutions is expected to last no more than two years, and thus we expect to have multiple hiring cycles for the duration of this project.

Table of Contents

1. Background/Introduction

The first wall and the plasma-facing components of the divertor are the first line of defense protecting the integrity of a magnetic fusion energy (MFE) reactor against the extremely harsh conditions of heat flux, neutron irradiation, thermal gradients, and tritium buildup and retention expected during device operation. The current lack of facilities to test materials and reactor components under representative fusion reactor conditions calls for the development of accurate numerical models capable of predicting the performance limits of materials and components under steady-state operation and transient events. While several first wall and divertor concepts are under consideration by the MFE community [1-7], those based on tungsten as an armor material are the most promising in terms of withstanding operational heat fluxes under long-pulse conditions (100s of seconds) required for a fusion pilot plant (FPP). In the first wall, tungsten is bonded to the tritium-breeding blanket of the reactor, which is generally supported by a He-cooled substructure made of a fusion-grade steel (such as a reduced-activation ferritic/martensitic, or 'RAFM', steel) enclosing the breeding element. In liquid breeders, the structural RAFM is protected by SiC flow channel inserts that also act as a tritium permeation barrier. In the divertor, the tungsten monoblock design has become the leading candidate for demonstration reactors and involves a tungsten armor block bonded to a fusion-grade copper alloy (such as Cu-Cr-Zr or 'CCZ') cooled by either helium (US concepts) or water (international concepts) [4,8-11]. Safe and reliable operation of an FPP requires a detailed understanding of the thermomechanical loads in these structures under operation so that accurate component lifetime limits can be established.

Thermomechanical modeling fusion reactor structures is extremely challenging. In the ThermChem-FW Center, we will focus on the first wall/blanket (FW/B) structure, with the divertor potentially becoming the focus of future proposal renewals. As noted above, the FW/B element involves several material systems performing distinct functions and separated by multiple interfaces. Integrated models must therefore consider (i) a large database of material properties, (ii) a wide geometric design space, (iii) processes governed by very disparate spatiotemporal scales, and (iv) a complex dynamic evolution resulting from the interplay of various operational variables, often affecting one another in intricate and nonlinear ways. Despite important efforts [12-19], the fusion community still lacks accurate models that capture the full thermomechanical response of the FW/B structure dynamically, i.e., as a function of reactor operational time (subsequently also referred to as 'burnup', 'dose', or 'fluence'). This time dependence emerges from two main materials aspects. First, a varying chemical and isotopic composition and gas atom buildup directly related to neutron transmutation. Second, microstructural evolution occurring as a response to severe operational conditions such as high temperatures, neutron irradiation, mechanical loads, and a complex internal chemistry (including corrosion) [20,21]. These processes include hardening, swelling, thermal and irradiation-induced creep, embrittlement due to the buildup of gaseous and solid transmutants, and grain growth and recrystallization.

2. Project Objectives

The framework described above represents a new paradigm where fundamental material properties, microstructure-property relations, and component-level thermomechanical behavior cannot be accurately assessed solely based on 'zero-point' considerations (i.e., time-fixed starting assumptions). We propose to address this knowledge gap by developing large-scale computational methodologies bridging the scales over which fundamental material property changes take place —at the atomic level— with where macroscopic-level evaluations can be made —at the component scale—, all within the context of realistic fusion operation conditions.

This undertaking constitutes an effort of grand challenge proportions, where both existing and new simulation techniques must be expanded and developed to accurately capture this complex time-evolving picture. At the same time, appropriate numerical and computational tools must go hand-in-hand to (i) expand the applicability of material models to device-representative geometries consisting of millions of degrees of freedom, and (ii) propagate uncertainties from the atomic scale up to microstructural and component-level models so that useful lifetime and failure estimates can be quantitatively defined.

In short, the main objective of this proposal is to develop an integrated computational model linking the materials physics scale with the component-level scale to simulate the thermomechanical response of the FW/B structure during operation conditions representative of FPP concepts.

In association with the above technical goals, workforce development by training graduate students and postdoctoral researchers in the fields of computational materials science and applied math applied to fusion energy will also be a priority objective of this proposal.

3. Proposed Research and Methods

3.1 Technical project structure

The materials physics scale must capture property changes due to nuclear transmutation and irradiation damage, and an evolving microstructure due to the onset of incubation phenomena such as swelling, creep, and recrystallization. To link these physics with the component-level response, we propose a three-level breakdown of the spatiotemporal scales of the system, each one addressed by scale-relevant computational modeling and applied mathematics tools. Levels are connected to one another by bi-directional information channels passing data, codes, and uncertainties in the model predictions.

1. Level 1 captures atomic-level physical processes reflective of fusion reactor operation in the FW/B structure, such as (i) transmutation, primary knock-on atoms (PKA) distributions, (ii) cascade damage, (iii) interactions of defect clusters, and (iv) tritium uptake, trapping, and diffusion.
2. Level 2 operates at mesoscopic scales where microstructural evolution occurs, including irradiation hardening, irradiation creep and swelling, thermal fatigue, precipitation, recrystallization (grain growth), and tritium permeation and retention. Uncertainties passed from Level 1 will be incorporated into model predictions to define confidence intervals and boundaries.
3. Level 3 involves time-dependent simulations using the finite element method (FEM) of the thermomechanical evolution of the full FW/B structure. These models will capture the entire geometric complexity and diversity of the multi-material FW/B and will furnish component lifetime prediction and design recommendations based on stress distributions and material property degradation. Uncertainties passed from Level 2 will be incorporated into model predictions to define confidence intervals and boundaries.

The novel developments proposed here with respect to standard thermomechanical performance and design codes include: **for Level 1**, time-dependent PKA energy distributions, cascade damage, and defect cluster structures due to isotopic inventory evolution from transmutation; **for Level 2**, microstructural evolution models formulated to reflect the time-dependent nature of fusion reactor operation (i.e., accounting for changes in defect concentrations, dislocation densities, grain sizes, and grain boundary sink efficiencies); **for Level 3**, the introduction of time-changing material constants and reduced parameter descriptions of materials evolution into component-level simulations with full spatial and temporal resolution.

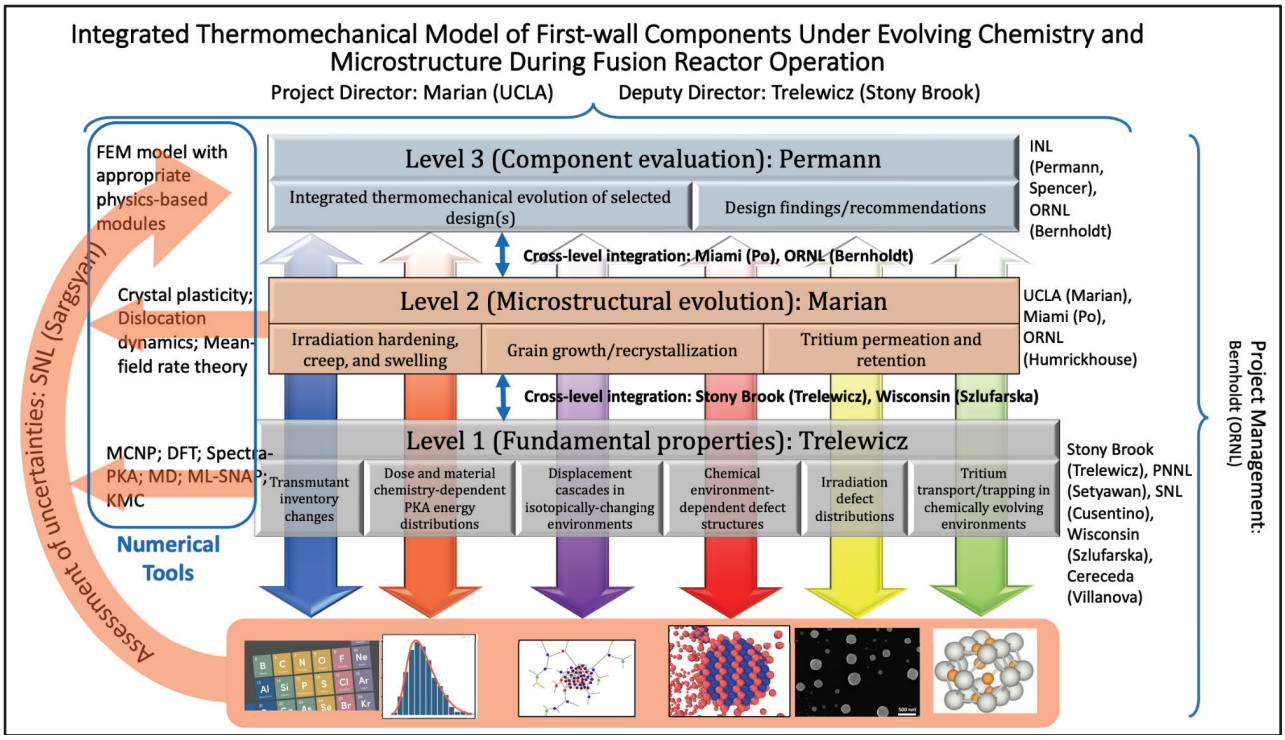

Figure 1: Management structure of the project, showcasing the subdivision of tasks into three levels: 'Level 1' (bottom level) will furnish fundamental material properties as a function of 'burnup'; 'Level 2' (intermediate level) captures microstructural evolution at mesoscales and provides constitutive relations; the boundary value problem is represented by 'Level 3' (component level, continuum scale), which yields the overall thermomechanical response of the device. The figure also shows the different personnel ascribed to each level and their interconnectivity, which has been designed to facilitate flexibility and adapt quickly to changes in project direction due to new information or unexpected difficulties.

A diagram describing the technical structure of the project is given in Figure 1 (the management structure, also included, is discussed in Section 4.1). The figure shows the integration among the three scale levels, indicating the tools, processes, and co-PI expertise. It is important to emphasize that the main novelty of this proposal will be the development of physics-based, time-dependent capabilities and their integration into thermomechanical evolution models. As will be discussed in Section 3.5, we will explore three simulation scenarios: (i) the FEM simulations (Level 3) will directly run microstructural submodels (Level 2) at the nodal level simultaneously using suitably designed libraries parametrized and verified by physics simulations at Level 1; (ii) FEM simulations will run physics-based constitutive models (based on Levels 1 and 2), developed independently, and (iii) using neural networks to subsume complex multidimensional state variable dependences into reduced-order models that can be run on the fly. Validation, while challenging, will be sought at the level of each individual model task before it is marked as ready to be passed to and/or used in higher-level models.

3.2 Reference component geometry

In this proposal, we consider a reference design for the first wall building block as a test bed for our material models using standard dimensions published in other studies. In ThermChem-FW, we will consider the geometry shown in Figure 2, which is representative of the FW/B design in reactor concepts that will bridge ITER with a future FPP, i.e., such as DEMO and FNSF (*Fusion Nuclear Science Facility*). The figure shows the frontal element of a liquid-metal breeding blanket concept, from the plasma edge to the breeding module just before the support backplates. This design consists of a thin W armor plate bonded to a structural RAFM steel that supports the flow channel insert through which liquid Li-Pb flows. The steel structure is actively cooled by He

channels flowing through its front side, as indicated in the figure. As a representative RAFM material, we will first focus on F82H [22], with consideration of other alloys in later stages of the proposal as discussed in subsequent sections.

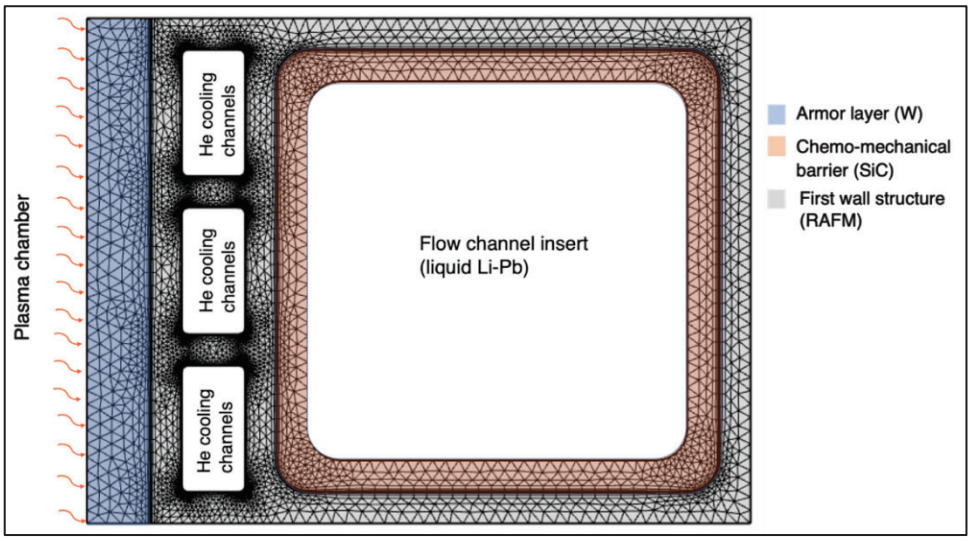

Figure 2: Schematic geometry of the reference FW design considered for the material models in this proposal. The figure represents a first wall frontal section containing the breeding element.

While this geometry is typical of concepts being considered by the MFE community, we emphasize that the focus in this proposal is not to endorse or validate this or any other specific first wall/blanket designs, but to develop advanced simulation methodologies that could be used for design optimization and comparing performance predictions among different designs for selection purposes.

3.2.1 Neutronics calculations (Task 1.0)

A previously developed model of the FNSF plasma source and geometry [23] will be used with existing parametric geometry tools to create a neutronics model of the reference component geometry using MCNP6.2 [24] and DAGMC [25]. These codes will be used to compute the volumetric heat generation rate, volumetric tritium production rate, and neutron flux and energy spectrum, tallied directly on an unstructured finite element mesh. The latter information will be passed to the FISPACT-II code [26,27] to compute transmutation product inventories as a function of time and radiation damage rates (discussed in Section 3.1.1).

3.3 Level 1: Time-dependent material properties from atomistic scales

The focus of the research at the atomistic level is to build a fundamental understanding of the atomic-scale mechanisms driving property changes of first wall materials over time due to the combined effects of radiation damage and transmutation. The task flow for the Level 1 activities is outlined in Figure 3. The different activities are organized into three main thrusts (colored in blue, orange, and red), which are described in detail in the sections that follow.

3.3.1 Transmutation rates and PKA energy spectra (Task 1.1)

During transmutation, nuclear reactions take place that alter the nuclide composition over time. Given the guiding FSNF blanket configuration shown in Figure 2, we will consider the most important transmutants in each material, i.e., Re and Os in W [28]; H, He, and Mn in the RAFM steel [29], and He and Mg in SiC [30,31].

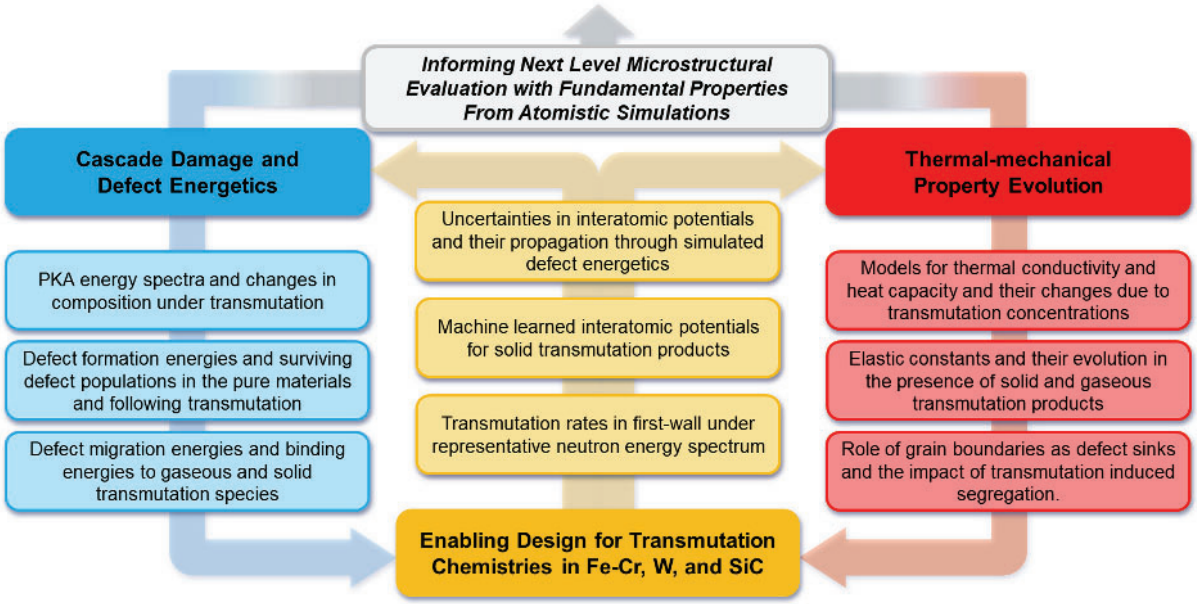

Figure 3: Overarching task flow and technical milestones for Level 1 atomistic scale modeling combining FISPACT-II, SPECTRA-PKA, FitSNAP, DFT, and MD codes with BTE modeling for thermal properties. Uncertainty quantification will be incorporated within ML-IAP and propagated through MD simulations.

Our approach to understanding how the W, RAFM, and SiC materials evolve their chemical composition over time is to use the FISPACT-II inventory code with the latest TALYS-based Evaluated Nuclear Data Libraries [32]. We will numerically solve the set of coupled differential equations that describe the rate of change of all possible nuclides and thus evolve the nuclide composition in time [33]. Members of the ThermChem-FW team have experience executing these calculations [34], as exemplified in Figure 4a for W under DEMO-FW conditions.

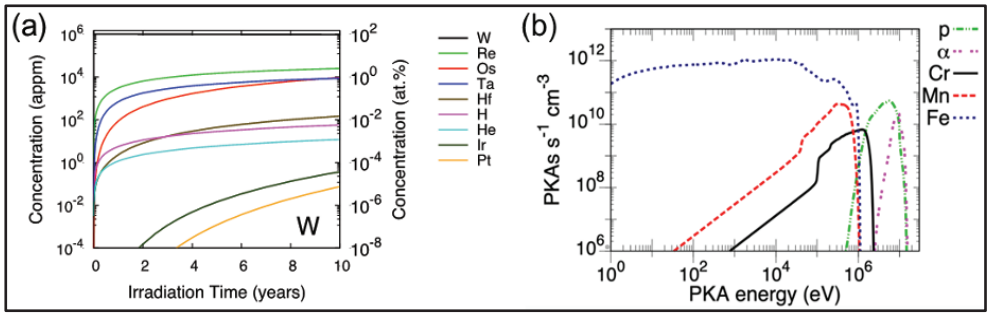

Figure 4: (a) Transmutation of W after 10 years of continuous exposure to DEMO conditions [34]. (b) PKA distributions for pure Fe under DEMO FW conditions [26].

The results of the inventory codes will provide a detailed sequence of the time evolution of nuclide concentrations in the three candidate materials under the expected conditions of FNSF. This evolving chemistry will also be used to update the underlying primary knock-on atom (PKA) energy distributions. For this purpose, we will employ the SPECTRA-PKA code [35,36], which combines neutron spectra with nuclear recoil data from nuclear data libraries to produce PKA spectra for any material composition. The expected outcome is a calculated database of the initial primary disruptions in W, RAFM, and SiC with information about the type, energy, and spatial distribution of the PKA. Such information, as shown in Figure 4b for pure Fe also under DEMO FW conditions [26], will be used to inform upper-level modeling within this project to investigate cascades with full atomistic interactions.

3.3.2 Machine learned interatomic potentials and uncertainty quantification (Task 1.2)

Within the multiscale hierarchy proposed in this work, it is critical to have access to highly accurate atomistic models to reduce error propagation into the higher length scale models. Classical potentials are often not transferable to conditions beyond what they were fit for, notably in far-from-equilibrium conditions such as in the FW/B. Recently, a new class of machine learning interatomic potentials (ML-IAP) [37-40] has emerged that are trained to large datasets of density functional theory (DFT) calculations, allowing for quantum accuracy with MD scalability [41]. One such ML-IAP, the *Spectral Neighbor Analysis Potential* (SNAP) [40], has been successfully used for materials [42-44] in fusion relevant scenarios (e.g., Be and He implantation at the plasma-material interface of a tungsten divertor [45-47). Recent updates to the fitting software, FitSNAP [48], allow for even more options and flexibility in fitting more complex models such as Atomic Cluster Expansion (ACE) descriptors [49] for treating each *n*-body term as a separate basis expansion allowing for tailoring of the different bonding descriptors. Additional models for magnetism [50] are available in LAMMPS [51] and can be coupled with SNAP [52] for including magnetic effects. This will be especially important for developing Fe-Cr ML-IAP, as magnetic effects may be important during reactor operation. To arrive at IAP predictions with *quantified uncertainties*, members of the ThermChem-FW team have recently implemented FitSNAP solvers, i.e., fitting procedures, that rely on Bayesian regression with embedded model error estimation [53] leading to SNAP ML-IAPs with augmented uncertainties. UQ enables variance decomposition based global sensitivity analysis (i.e., allowing extraction of descriptor importance indices), active learning (i.e., selection of DFT training sets to maximize the efficiency of ML-IAP construction), as well as uncertainty propagation when SNAP ML-IAPs are fed into MD simulations. Additional solvers, like high-capacity neural networks (NNs), are also now part of the FitSNAP package. Unlike linear or quadratic SNAP forms, UQ tools with NN-based ML-IAPs are less mature, largely relying on empirical sampling methods for assessing uncertainties. In cases where such ML-IAP forms are necessary, we will rely on our recent work and in-house software [54], bridging state-of-the-art UQ tools and empirical methods to reliably arrive at NN-based ML-IAP uncertainty estimation.

In this project, the ThermChem-FW team will develop a set of ML-IAP for FW/B materials with a focus on capturing the effects of transmutation on defect diffusion and trapping, and in the values of the elastic constants and thermal conductivity. This will be achieved by developing specific ML-IAP for W-Re-Os, SiC-Mg, and Fe-Cr-Mn/He with the latter system incorporating magnetic contributions, which represent a current gap for modeling radiation effects in Fe-Cr. A set of DFT training data will first need to be developed that includes configurations relevant to the application such as defect structures, elastically strained unit cells, high temperature DFT-MD, etc. The general procedure is summarized in Figure 5. DFT simulations described in subsequent sections for each material system free of transmutation species will be leveraged as training data. Potentials will be optimized to reproduce key material properties like defect formation energies and elastic constants. Initially, SNAP with linear regression will be

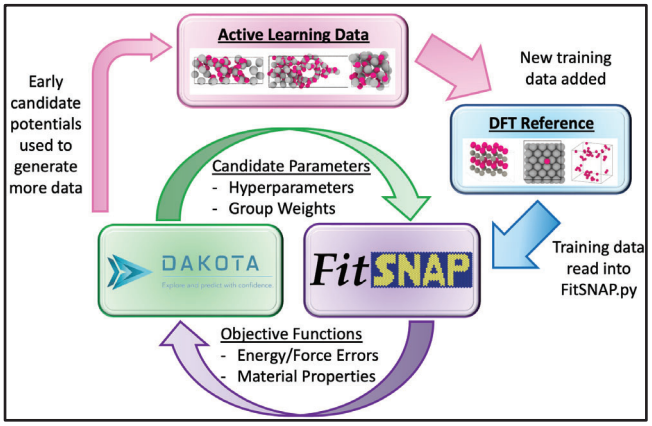

Figure 5: ML-IAP development employing DFT reference data and active learning with ML loop

employed with magnetic models incorporated for Fe-Cr; NN-SNAP or ACE can also be used as needed. With SNAP, well-established UQ tools such as polynomial chaos (PC) expansions [55] will be implemented to describe input parameter uncertainties from UQ-SNAP solvers and propagated through MD simulations. Overparameterized models, such as neural networks, may not be amenable to PC treatment and will be supplemented by standard Monte-Carlo UQ.

Potentials will be optimized using the genetic algorithm capability within the Dakota software, which has been used for previous SNAP development with predefined material properties targeted as optimization parameters. The UQ-augmented ML-IAP will be validated against DFT and/or literature data using established metrics for probability density function comparison in case data comes with uncertainty estimation or likelihood functions if reference values are given as point estimates. We will use judiciously selected ML-IAP samples from UQ-FitSNAP solvers to perform MD simulations to predict the effect of transmutation on defect transport, elastic constants, thermal properties.

3.3.3 Cascade damage and defect energetics (Task 1.3)

Defect production as a function of evolving chemistry and microstructure due to neutron irradiation serves as a critical input to the microstructural scale modeling and necessitates a mechanistic understanding of the atomistic scale defect characteristics and energetics [56-60]. An evolving internal chemical composition has been shown to influence both the numbers of primary cascade defects as well as their type and size distribution. MD studies have indicated that the composition of defect clusters under a changing chemical inventory is typically different from the composition of the material. For example, in W-5%Re, the interstitial clusters typically contain ~10% Re [61]. In SiC, interstitial clusters contain ~80% C [62], while significant enrichment of Cr is observed in the interstitial clusters in Fe-Cr [63].

In this task, we will study the effect of evolving chemistry on defect production due to changing PKA energy distributions. First, we will continually update the PKA energy distributions as a function of the concentration of the transmutation products to be included for each material (see Section 3.1.1). Suitable damage functions that relate the number of defects to the PKA energy will be constructed and updated as a function of burnup as well [36]. Then, a selected set of cascades with the different PKA types in each material will be simulated via MD using LAMMPS with the corresponding ML-IAP. From these simulations, we will generate three to five datasets of cascades to cover the expected range of composition (likely a few atomic %), with additional datasets generated as needed. Combined with the cascade simulations will be the calculation of defect formation energies using DFT considering point defects and defect clusters in the presence of transmutation products as a function of concentration and compared with the energetics from MD to verify the accuracy of the ML-IAP while also providing input to the active learning loop.

For the calculations of defect kinetics in the presence of transmutation impurities, we will treat the single crystal case as a representation of intragranular behavior since grain boundaries serve as sinks for defects. The main migrating defects that will be evaluated will include monovacancies, H (and T), He, He clusters, self-interstitial atoms (SIAs), SIA clusters, and solid transmutation products. For point defects and simple clusters, DFT will be used to compute the migration energies using the climbing nudged elastic band method [64]. The attempt frequencies in the diffusion prefactors will be calculated using harmonic transition state theory. Zero-point-energy corrections will be considered for light isotopes, such as H and T. For extended defects, the diffusion coefficients will be derived from Arrhenius plots obtained from MD or kMC simulations [65]. We will employ parallel replica and/or other accelerated MD (AMD) techniques for slowly diffusing species (e.g., as previously performed by ThermChem-FW team members to

determine the mobility of small interstitial clusters in SiC [66]). A nuance for SiC is the charged nature of the defects, which necessitate consideration of the most stable charge state and the dependence of the Fermi level on transmutation impurities. The Fermi level in SiC will be determined as a function of concentration for the dominant transmutation products.

Literature data (e.g., W [67,68], Fe-Cr [69-71], SiC [72-75]) will be combined with calculations using the ML-IAP to map the migration kinetics and the effects of the solid transmutation products as well as other defects influenced by shifts in local chemistry. Even where data is available based on empirical potentials, the ML-IAPs can improve upon the accuracy of these datasets (as, e.g., in the diffusion coefficients of He clusters in W [76] and Fe [77]). Existing data on vacancy migration typically does not consider the effect of transmutation, which will be addressed in this task via MD to derive the effective diffusion coefficients of monovacancies as a function concentration. In the dilute limit, DFT can also be used to compute vacancy diffusion in the presence of substitutional solutes (likewise vacancy-mediated solute diffusion) by using a multiple-jump-frequency model [78]. We will also compute the diffusion kinetics of intrinsic and transmutant interstitial defects. In W and Fe-Cr, interstitial solutes are most stable in a mixed dumbbell configuration, which migrates via translation and rotation [79,80]. While the rotation barrier for mixed dumbbells is usually known, that of SIA clusters especially in the presence of solute is less understood. Our study will therefore compute the rotation kinetics for SIA clusters in W and Fe using ML-IAP.

For defect trapping, we will consider SIA and vacancy clusters and their binding to transmutation products. Our team has experience doing these calculations for the binding of defects to fission products (i.e., Ag, Cs, O, and I) in SiC [81]. The energy landscape of defect clusters can be complex and, in some cases, identifying clusters with the lowest energies can be computationally challenging. To address this issue, a genetic algorithm will be implemented to optimize structures in SiC, bcc Fe, and bcc Fe-Cr alloys [82]. We will leverage those results and extend the methods to identify stable clusters in the presence of transmutation products. Additionally, special consideration will be given to He, which aggregates to form gas bubbles in the lattice or at grain boundaries. In particular, here we will focus on the accumulation of He in the lattice, both in W and Fe [83-88], where bubbles can adopt various geometric shapes which determine their stability [89-91]. Here, literature data will be leveraged in conjunction with high-temperature MD simulations of different He/V ratios and different initial structures that include the presence of transmutation products. An important outcome of this thrust will be the calculation of bubble energies as a function of bubble size and He/V ratio, which will be used to extract binding energies of He, vacancies, and transmutation products to the bubbles.

3.3.4 Evolution of thermal-mechanical properties with transmutation (Task 1.4)

Thermal conductivities, elastic constants, and coefficients of thermal expansion (CTE) are essential properties for fusion component design and can be significantly altered by the combined effects of radiation damage and transmutation products [92,93]. In this task, coupled DFT, MD, and Boltzmann Transport Equation (BTE) modeling will be leveraged in concert to estimate changes in the thermal conductivities and elastic constants as a function of evolving chemistry due to transmutation.

Thermal conductivities (κ): These will be calculated following an *ab-initio*-informed semiempirical approach developed by members of the ThermChem-FW team. The approach has already been demonstrated for metallic uranium fuels [94-97] and provides accurate models with limited experimental data and significant insights into the physics of various electron- and phonon-scattering mechanisms. To begin, we will assume a single-phase element or alloy with known electrical/thermal conductivity data and crystal structures for DFT calculations. In the DFT-BTE

approach, DFT calculations are used to calculate the structural, electronic, and vibrational properties while BTE modeling calculates transport properties such as electrical/thermal conductivity, based on inputs from the DFT calculations. Parameters that are difficult to obtain accurately from DFT, such as electronic and phonon relaxation times, are modeled via either semi-classical physics formulae or empirical fitting and categorized according to the different electron- and phonon-scattering processes involved. For general single-phase materials, we can write the thermal conductivity, κ, in the non-radiative transport regime as sum of the electronic thermal conductivity, κ_e, and phonon thermal conductivity, κ_{ph}, and then use the Wiedemann-Franz law, BTE, and Matthiessen's rule [98] to obtain the relations:

$$\kappa = \kappa_e + \kappa_{ph} = \frac{L}{T\rho} + \frac{1}{3\Omega N_k}\sum_{k\lambda}^{N_k} c_{k\lambda} v_{k\lambda} \otimes v_{k\lambda} \tau_{k\lambda}^{ph} \quad (1)$$

where L is the Lorenz number, k is the wavevector, λ is a specific phonon branch, N_k is the total number of discrete k-points, Ω is the volume of the unit cell, and $c_{k\lambda}$, $v_{k\lambda}$ and are $\tau_{k\lambda}^{ph}$ the heat capacity, phonon group velocity, and phonon relaxation time for each wavevector k and phonon branch λ, respectively. $\tau_{k\lambda}^{ph}$ includes the effect of scattering processes with other phonons, electrons, point defects, grain boundaries, or dislocations, all of which can be obtained using DFT calculations [99-101]. The electron and phonon BTE calculations will be performed using the BoltzTraP [101] and Phono3py [102,103] software, respectively, along with the relaxation time approximation and available electrical and thermal conductivity data extracted from literature. An example of the effectiveness of this approach for U and Zr is show in Figure 6 [97]. We expect to focus on a limited set of transmutation products as noted at the outset of this task but span all the relevant first wall materials (i.e, W, each sublattice in SiC, and three compositions of Fe-Cr). As well, our results will be compared to existing calculations and experiments [104-106].

Elastic constants (C_{ij}): We will use DFT calculations to update the values of the elastic constants C_{ij} with chemical inventory composition by evaluating the change in the total energy per unit volume ($\Delta U/\Omega$) of a system subjected to a general deformation: $(\Delta U/\Omega) = ½C_{ij}u_iu_j$, where Ω is the volume of the unit cell, C_{ij} is the elasticity tensor, and u_j are the engineering strain vectors. Other elastic properties of interest, such as the bulk and shear moduli or Poisson's ratio, will be directly extracted from C_{ij} to be used in Level 2 and 3 simulations. The elastic properties of isotropic polycrystalline materials will also be determined by using the Hill average and the Voigt and Reuss bounds with complementary MD simulations.

Thermal expansion coefficients (α_V): CTE will be obtained for all materials by performing MD simulations under the isobaric-isothermal (NpT) ensemble. The simulations will be conducted at different temperatures using simulation cells sufficiently large to capture representative chemical compositions due to transmutation as a function of burnup. While maintaining a zero-pressure condition, the converged (steady state) value of the cell volume will be recorded and the CTE will be obtained as $\alpha_V = \frac{1}{V_0}\left(\frac{\partial V}{\partial T}\right)_p$ —where V_0 is the relaxed cell volume at 0 K— from a set of independent constant-temperature simulations [107].

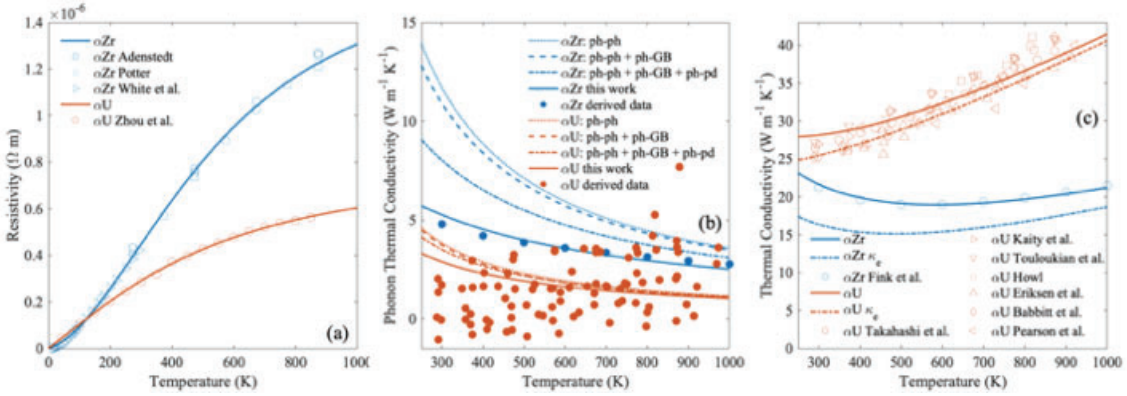

Figure 6: Selected examples of thermal properties calculated using the proposed framework including (a) resistivity, (b) phonon thermal conductivity, and (c) total thermal conductivity for α-U and α-Zr [97].

3.3.5 The role of transmutation induced segregation on grain boundary sinks (Task 1.5)

In certain materials, transmutation products will have an energetic preference to segregate to grain boundaries (e.g., Re/Os in W [108-110]) rather than stay as crystal solutes. This has two implications. First, the preferential diffusion of transmutation products to the grain boundaries (GB) can influence the surviving defect distribution within the lattice, particularly when they bind to impurities species. Second, the preferential occupation of grain boundary sites by transmutation products can impact their sink strength relative to the pristine grain boundary distribution. With the first mechanism addressed through the analysis of the binding energies of different defects to impurity species under Section 3.1.3, the effect of transmutation-induced grain boundary segregation on the interaction with radiation induced point defects and defect clusters will be quantified under this task.

For each of the first wall materials, the propensity for different transmutation impurities to segregate to grain boundaries system will be quantified using a simulated polycrystalline structure with random texture constructed using a Voronoi tessellation procedure [111]. Impurity atoms will be introduced by randomly substituting host atoms on the crystalline lattice, and the hybrid molecular dynamics/Monte Carlo (MD/MC) approach [112] will be used to achieve energy minimized structures with respect to structural relaxations, thermal vibrations, *and* chemical mixing. In cases where segregation of transmutation products is identified, simplified bicrystal grain structures with coincident site lattice (CSL) boundaries containing systematic variations in their energy, degree of symmetry, and excess free volume will be constructed and energy minimized to produce different extents of grain boundary segregation. Changes in the sink strength will be assessed by updating the capture efficiency of the GB over time, which can be expressed as the ratio of the lifetime of SIA and vacancy defects near a pristine GB relative to that of a solute-segregated GB [113-116]. The updated capture efficiencies will be used to inform our mesoscale irradiation models described in Section 3.4.1. A similar approach will be undertaken to calculate the interfacial rate constants needed for the tritium retention model in Section 3.4.3.

3.4 Level 2: Microstructural evolution models and the 'micron' scale

This level consists of a centralized irradiation damage module that takes information from Level 1 and feeds into three microstructural evolution submodels:

I. Irradiation hardening and creep: these phenomena define the lower and upper temperature operating window of structural materials, respectively [117,118]. We will develop a dislocation-density-based Crystal Plasticity (CP) model that accounts for both phenomena,

whose state variables are taken from the centralized irradiation damage module, and that feeds back to that module in order to capture dislocation-irradiation defects interactions.

II. Grain growth and recrystallization: Tungsten is known to undergo recrystallization/grain growth (RX/GG) at critical combinations of irradiation dose and temperatures [119-125]. These processes must too be captured at the microstructural level, over grain-size scales. Here, we will develop a RX/GG model for polycrystalline W that reflects the operational conditions of a fusion reactor.

III. Tritium transport and retention: tritium can be directly implanted at small depths into the plasma-facing wall and is produced directly in the breeding zone behind it. This tritium can migrate throughout the structure (and into the coolant) via diffusion but will be retained at trap sites with a density and energy dependent on the density and type of defects induced by plasma exposure and neutron irradiation.

3.4.1 Centralized irradiation damage module (Task 2.1)

Fusion environments present a tremendous challenge in terms of irradiation damage accumulation models for three main reasons: (1) the existence of multiple defect and transmutation species during irradiation under fusion conditions leads to the exponential growth of coupled ordinary differential equations (ODE), which makes standard (deterministic) rate theory models impractical from a computational standpoint [126,127]; (2) ODE systems representing irradiation species accumulation in fusion environments are strongly coupled (all defects react with one another), leading to dense coefficient matrices that are significantly more costly to solve by direct methods than sparse systems [128,129]; and (3) these ODE systems are intrinsically stiff due to the large intrinsic variability of time scales representing each defect type. This led to the development of the Stochastic Cluster Dynamics (SCD) model [130,131], which avoids these limitations by casting the standard ODE system into a set of stochastic differential equations that can be solved using the residence-time algorithm [132]. For these reasons, SCD will be the irradiation damage simulation module of choice used in Level 2. In this project, we will consider vacancies, self-interstitial atoms, He atoms, H atoms, and the main transmutant elements in each material, identified in Section 3.1.1. Nonetheless, SCD will require computational developments to scale on large unstructured meshes. To that end, (i) we will consider

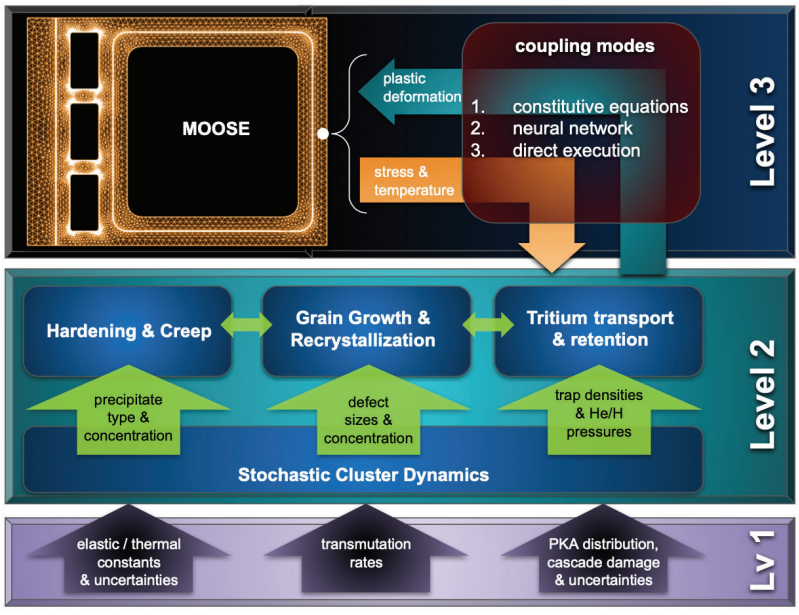

Figure 7: Internal arrangement of efforts for Level 2. Information from Level 1 into Level 2 is parsed by a common submodule based on the *stochastic cluster dynamics* code (SCD), which simulates the evolution of irradiation damage accumulation at a material point. The three microstructure submodules receive information directly from SCD, and are thus synchronized in time by the common input they receive.

machine learning-assisted evolution approaches for defect size predictions to accelerate SCD, as ThermChem-FW team members from PNNL have done to predict grain structures in metallic nuclear fuels [133], and (ii) we will explore parallel synchronization strategies between SCD and deterministic solvers following similar work done by UCLA [134,135].

The irradiation damage module sits atop and is common to the three microstructural models. This centralized approach achieves two important features. First, it connects all microstructural evolution (as modeled by submodels I-III) by providing common information to all four submodels, which makes them mutually consistent. Second, the irradiation module itself becomes updated by results furnished on the fly by the submodels, such that they all evolve in sync as dictated by microstructural change predictions. In particular, the following parameters of the SCD simulations will be updated on the fly (i) dislocation densities furnished from submodel I (irradiation hardening and creep) as evolving sinks for defects; (ii) grain size and grain boundary misorientations from submodel II to define sink strengths for defects; and (iii) tritium concentration profiles from submodel III to inform SCD distributions of vacancy-tritium clusters. This substructure and coupling of models in Level 2 is shown schematically in Figure 7. A technical description of each submodule follows.

3.4.2 Irradiation hardening and creep (submodel I, Task 2.2)

The irradiation hardening and creep model implemented at Level 2 is a dislocation-based polycrystalline crystal plasticity (PX-CP) model for irradiated bcc materials. The model follows recent developments done by the Miami and UCLA PIs [136] and is based on prior work by Patra and McDowell [137]. The model receives irradiation defect densities directly from SCD as described above and is connected to the grain growth and recrystallization module proposed in Section 3.4.2 by considering the effects of grain boundaries and the evolving grain microstructure. In particular, given a certain grain size distribution, we will render a periodic polycrystalline grain microstructure/texture to be used as the representative volume element (RVE) for hardening/creep simulations. Internally, a dispersed barrier model will be used to compute the athermal slip resistance on each slip system [138], as done in past works [139]. The dispersed barrier model includes contributions from the irradiation defects number densities and sizes computed by the SCD module, long-range contributions from dislocations and grain-boundary pileus, as well as the Peierls stress contribution proper of bcc metals. Preliminary hardening calculations based on a similar plasticity model coupled to SCD, as well as comparison to experiments [140], are reported in Figure 8.

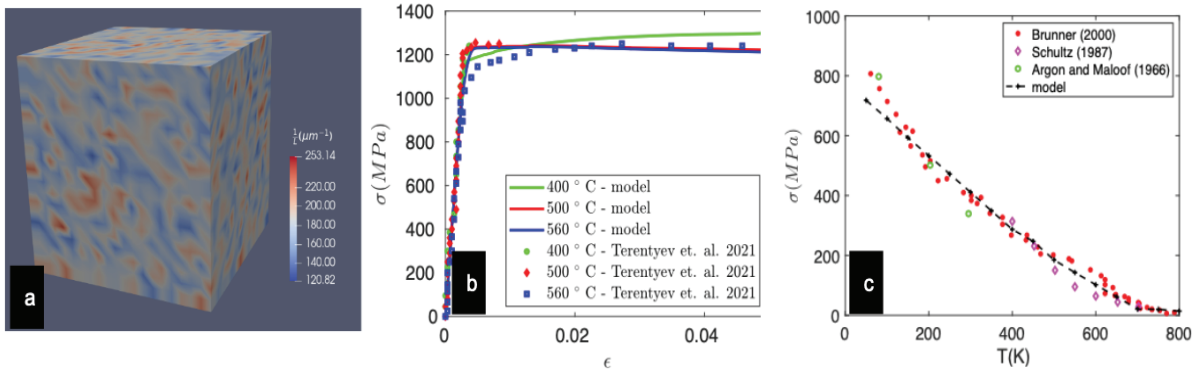

Figure 8: (a) Spatial distribution of irradiation hardening parameter. (b) Model comparison with experiments in irradiated W [140]. (c) Temperature dependence of the yield strength in pure W compared to experiments [141-143].

3.4.3 *Grain growth model (submodel II, Task 2.3)*

The RX/GG model builds on methods previously developed by the PI and others [144,145]. Grain boundary dynamics follows a linear viscous law such as: $v = Mf$, where v is the grain boundary (GB) velocity, M is the mobility, and f includes all the driving forces conducive to GB motion. Under the coupled effects of temperature and irradiation, grain boundaries can move due to curvature, differential plastic strain energy, and differential irradiation damage energy, i.e.:

$$f = -\gamma/R + Gb^2\Delta\rho + \Delta E_{dam} \quad (2)$$

where γ is the GB energy, R its curvature, G is the material's shear modulus, b is the Burgers vector's modulus, and $\Delta\rho$ is the dislocation density difference across the GB (resulting from plastic slip processes). The last term is the defect energy difference across the GB due to irradiation damage accumulation, which for each grain can be calculated as:

$$E_{dam} = \sum_\alpha \left[\int_1^N C_i \cdot e_i(n)dn\right] \quad (3)$$

α refers to the nature of the defects (vacancies, SIA, He or H clusters, transmutant atoms, etc.), C_i is the concentration of species i, n is the size of the cluster, and $e_i(n)$ gives the energy of a cluster as a function of n. Here, we will use $e_i(n) = e_0 n^{2/3}$, where e_0 is a constant.

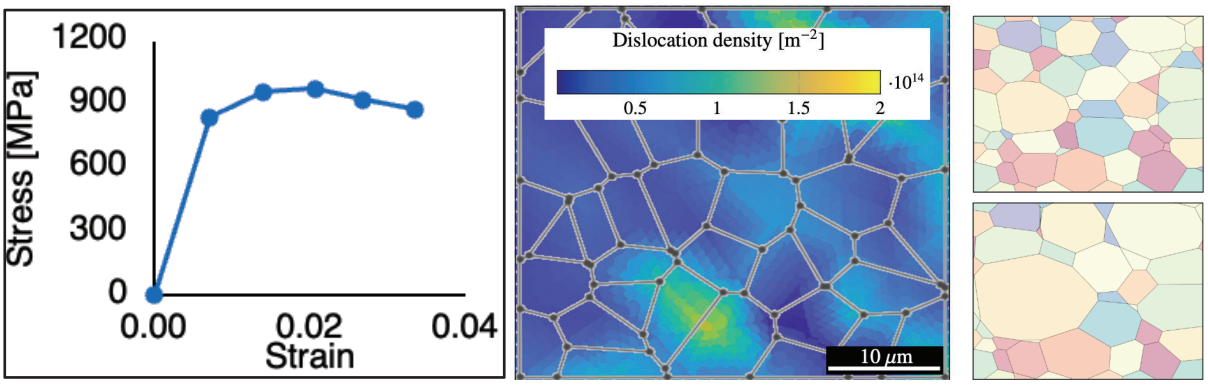

Figure 9: (Left) Schematic stress-strain curve for polycrystalline Fe. (Center) dislocation density buildup at the end of the deformation stage). (Right) Activation of grain boundaries at the critical temperature, leading to grain growth (from [144]).

Preliminary results for mechanically loaded Fe polycrystals are shown in Figure 9, where the connection between external stimuli (tensile loading in this case), the onset of a nonequilibrium metastable state (due to differential dislocation density buildup), and microstructural evolution (grain growth in that case) can be seen. Defect concentrations and sizes will be passed to the RX/GG model by the SCD module in 'real time', as well as dislocation densities from the plastic deformation module (see 3.2.1). $e_i(n)$, e_0, M and will be considered to be time-dependent parameters extracted from Level 1 at the atomic scale (Section 3.1). The RX/GG model will update the polycrystalline structure (grain shapes and sizes) to be passed to the higher scale (Level 3). Additionally, we will seek to explore the effect of selected dopants (primarily K) and transmutants (Re and Os) [123] on the predicted critical RX/GG temperatures at each irradiation dose point. Validation of the model will be sought by comparing against recent experimental results of grain growth in pristine and doped irradiated W-Re alloys [125].

3.4.4 *Tritium transport and retention model (submodel III, Task 2.4)*

To capture tritium transport, we will implement a standard diffusion/trapping model [146]. The concentration C of mobile tritium is obtained by solving a diffusion equation:

$$\frac{\partial c}{\partial t} - \nabla \cdot \left(D\left(\nabla c + \frac{Q^* c}{RT^2}\nabla T\right)\right) = S - \sum_i \frac{\partial c_{t,i}}{\partial t} \quad (4)$$

where D is the diffusion coefficient, T is temperature, R is the universal gas constant, and Q^* is the Ludwig-Soret coefficient. On the right-hand side, S is the local source or production rate, and $c_{t,i}$ is the concentration of tritium in trap i. Traps are associated with defect sites, and irradiation can create higher energy traps as well as an increased trap site density, with potentially significant implications for tritium retention and inventory. In this project, the trap concentrations (vacancy clusters, He/H bubbles) will be furnished directly by SCD, as indicated in Figure 7. At material/coolant interfaces, the net tritium flux J is given by the difference in competing dissociation and recombination rates, $J = K_d P - K_r c^2$, where P is the partial pressure of tritium in the coolant, and K_d and K_r are the dissociation and recombination rate constants, respectively. K_d and K_r both have an Arrhenius form and will be obtained from calculations as described in Section 3.1.5. Diffusion and Ludwig-Soret coefficients will also be obtained from Level 1 models. The source term on the plasma side will be defined as part of our collaboration with the future PMI-Scidac proposal selected for funding in this FOA (see details in Section 4.3).

3.5 Level 3: Full component thermomechanical simulations and integration of computational methodologies

The primary objective of the efforts at this level is to develop tools to predict the thermo-mechanical response at the component-level, integrating the mesoscale materials models with spatial resolution and time dependance. We will conduct full-component FEM simulations using the geometry provided in Figure 2 for the FW-B structure using FNSF-like conditions [5,16] to predict the integrity of the materials elements over time. Capabilities in multiple areas are needed to achieve this goal, as outlined below. MOOSE [147] will be used here as the component-scale multiphysics simulation tool, so these developments will be focused on expanding and improving upon the multiscale simulation capabilities in MOOSE and their interoperability with other tools. FEM simulations will use time-dependent material properties (elastic constants, thermal conductivities, and coefficients of thermal expansion) that reflect the evolving microstructure and material chemistry.

3.5.1 Interfaces between MOOSE and mesoscale models (Task 3.1)

A robust and flexible capability for capturing the physical behavior predicted by mesoscale models in component-level simulations is critical for the proposed multiscale simulation effort. A variety of physical phenomena will be considered in these mesoscale models, each with its unique features. To address the unique needs of each model type, support for the following types of multiscale coupling will be developed and applied in this project:

1. Closed-form expressions that represent the behavior of the lower-scale, high-fidelity physics models will be developed in cases where the predicted behavior has an obvious analytical form. This approach is typically most feasible when there are small numbers of inputs and outputs in the analytic reduced order model (ROM) and limited or no history dependence. Even when the model form is clear, obtaining the appropriate coefficients to calibrate those models can require significant effort, and the existing capability in the stochastic tools module (STM) [148] in MOOSE will be used to execute the lower-scale models and obtain optimal coefficients.
2. For constitutive relationships for which an analytical form is complex and the high-fidelity physics models are computationally expensive, neural network (NN)-based representations of the model are attractive alternatives. The NN-based ROMs can be directly used in the component-level simulation in place of the corresponding high-fidelity material models. This approach is particularly attractive for material models whose ROM is well-tested externally and/or the corresponding high-fidelity model is not compatible with MOOSE.

3. Finally, the component-level model can directly execute the high-fidelity model to obtain the response for material points in the component-scale model. This approach is generally most attractive for high-fidelity models with relatively low computational costs. A NN-based ROMs that represents the high-fidelity model can be used to accelerate that model by being used as a predictor for its solution. This indirect use of the ROM within MOOSE requires that the high-fidelity model is either a part of MOOSE or can communicate residual information with the ROM that is being used to represent it.

The integration of the three model interfaces just discussed is shown in Figure 7. A diagram of the ROM development and integration is shown in Figure 10.

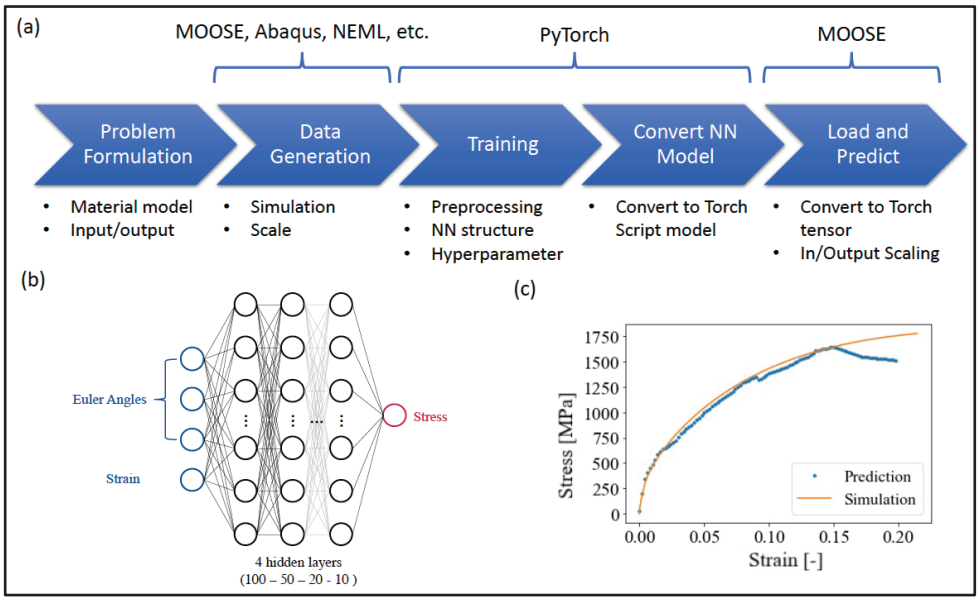

Figure 10. Integration of externally trained ROM in MOOSE. (a) Schematic of the ROM creation and its integration into MOOSE. (b) A crystal plasticity ROM represented by a fully connected NN that is successfully deployed in MOOSE. (c) Comparison between the ROM prediction and the ground-truth solution from the high-fidelity physics model.

An initial study has been carried out to demonstrate the successful deployment of an externally trained ROM within MOOSE. This project will further enhance this capability to ensure the success of having multiple externally trained ROMs work well together in MOOSE. Specifically, detailed standards for the ROM creation (e.g., structure, required package) will be discussed, documented, and distributed to collaborators upfront to avoid any potential compatibility issues. Meanwhile, a robust and versatile interface will be built within MOOSE to accommodate all possible ROMs needed for this project, which will come from a variety of codes, represent distinct constitutive relations, and operate on a variety of spatial and temporal scales. As described in the following sections, approaches to improve multiple aspects of the efficiency and accuracy of the NN-based ROMs used in the direct and indirect approaches will be developed in addition to the foundational support for multiscale coupling.

3.5.2 System for continuous online updating of reduced order models (Task 3.2)

Both the direct and indirect ROM approaches described in items 2 and 3 in the previous section will benefit from continuous improvement by providing updated data in the regimes for which they are applied. To continuously improve the ROMs, a recurrent training capability will be developed.Here, recurrent training refers to an online training process that utilizes information obtained during the ROM's application to improve its performance. To achieve this goal, an additional NN will be trained to provide corrections to the ROM's predicted response. This correction model takes the same input as the ROM (e.g., strain, flux, irradiation dose, etc.) and predicts the difference between the ROM prediction and the ground-truth response. The predicted correction is then added to the ROM prediction and acts as a final prediction. A diagram of this approach is shown in Figure 11. Despite the continuous training of the correction model as the ROM is being evaluated, updating the correction model for actual use will be infrequent. This is to avoid any potential instabilities that may be caused by the sudden change of the correction model. In this project, a tool for automating this online training, evaluation, and staging process will be developed in MOOSE. Note that this recurrent training capability will also need frequent forward evaluations of the material constitutive relation, which will require communication between MOOSE and the high-fidelity material constitutive relation.

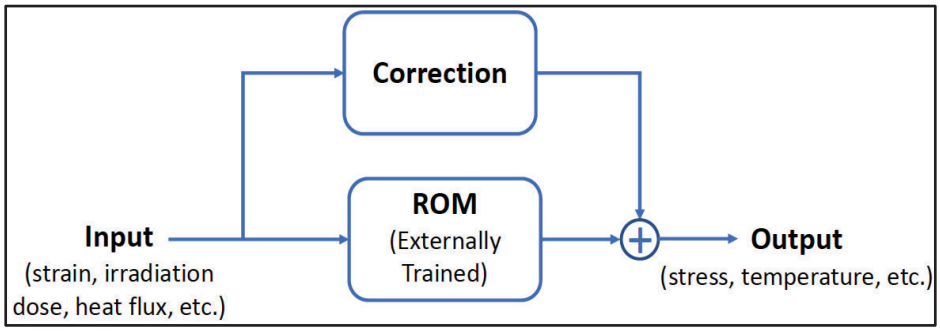

Figure 11: Schematic of the correction model for improving ROM performance.

3.5.3 Synchronous interaction between MOOSE and external applications (Task 3.3)

For instances when the codes used by the high-fidelity physics models for lower length-scale simulations are not based on MOOSE or readily able to be modified to be called by a MOOSE model, we will develop a web-interface-based capability for communication between MOOSE and that application. This will allow information flow from MOOSE to external applications and vice versa in a synchronized way, without the need to directly link the applications to MOOSE. This interface could be used to enhance reduced-order models derived from mesoscale simulations on the fly based on feedback from the component-based simulations. It can also enable the on-the-fly training of reduced-order models within external applications based on results and residuals inside the MOOSE component-level model.

3.5.4 GPU-accelerated machine-learning models in MOOSE (Task 3.4)

The scientific machine learning capabilities in MOOSE heavily rely on the open-source C++ front end (Libtorch) of PyTorch [149]. The current implementation is based on the CPU-based version of Libtorch and leverages the message-passing interface (MPI) for training NNs in parallel. The application of NNs for replacing computationally expensive material model evaluations on the meso- and component-scales is currently limited by the evaluation speed of the NNs, which can potentially be very large. Convolutional NNs connecting grain structures with material properties are a good example of NNs whose evaluation can be expensive. Another application of NNs is to use them as predictors for reducing iteration counts in complex material models. However,

this is only viable if the NNs can be evaluated rapidly. Libtorch has native support of GPU resources for the training and handling of a wide variety of NNs, which would be very beneficial for these demanding applications. GPUs are well suited for the evaluation and training of NNs due to their capability of tremendously accelerating dense matrix-vector operations. For this reason, we propose to develop interfaces and algorithms in MOOSE, which are able to seamlessly utilize GPU resources when available and fallback to CPU resources, when necessary, while managing NN-based material model evaluations. To the extent possible, these interfaces will abstract hardware details from the programming interface, allowing application developers to readily make use of the most advanced and appropriate hardware on a given machine. Additionally, the ability to force the selection of specific hardware will be made available for the purposes of drawing both speed and accuracy comparisons, troubleshooting, and other research-related purposes.

4. Management Plan and Timetable of Activities

4.1 Management structure

As indicated earlier, this project is structured as an assembly of three spatiotemporal levels connected through bidirectional information channels, each including both materials physics and computational/applied math subactivities. Level 1 (the *materials* level) encompasses physical information at the atomic scale and will be coordinated by Trelewicz (Stony Brook), with contributions from Szlufarska (Wisconsin), Setyawan (PNNL), Cusentino and Sargsyan (SNL), and Cereceda (Villanova). Information from Level 1 will be passed to Level 2, which will capture the microstructural scales (microns, milliseconds) through suitably developed mesoscale models. This level will be coordinated by Marian (UCLA), with contributions from Po (Miami) and Humrickhouse (ORNL). Information from Level 2 will be passed to Level 3, which will be defined by large-scale, component-level, finite element simulations to be carried out by Permann and Spencer (INL). Key personnel will be designated as liaisons between the different levels to ensure an efficient and accurate transfer of information. Trelewicz (Stony Brook) and Marian (UCLA) will oversee the connection between Levels 1 and 2, while Bernholdt (ORNL) and Po (Miami) will act as liaisons between Levels 2 and 3, while Bernholdt (ORNL), Spencer (INL), and Po (Miami) will also assist the team in the optimization of algorithms, parallel scalability, development of software interfaces, and overall methodology implementation. The variability of material properties due to uncertainties in density functional theory (DFT) calculations and experimental databases used to fit the interatomic potentials, and their effect upstream into the intermediate and top levels, will be assessed by Sargsyan (SNL: member of *FastMath*). The project director (Marian, UCLA) will be responsible for managing all tasks and activities within this proposal, with assistance from Trelewicz (Stony Brook) as deputy director, and Bernholdt (ORNL) as project manager. Figure 1 also contains an overall picture of the project's management structure, emphasizing the different connecting blocks and researcher attributions.

The team will hold bi-weekly progress meetings via Zoom, where preference will be given to students and postdocs to present their progress. As well, a ThermChem-FW 'retreat' will be organized yearly by one of the institutional PIs for the team to convene in-person and discuss results, progress, and team member productivity and well-being.

In case of a successful award, the project PI (Marian) will receive four quarters of teaching relief (one per academic year) from UCLA's School of Engineering so that he can devote the majority of his time to the performance of his technical and managerial duties under the ThermChem-FW project.

4.2 Proposal team

The team assembled to put the above plan into effect consists of a blend of computational materials scientists ('Mat Sci') and applied math/computer scientists ('Comp Sci') working in an integrated fashion. As Figure 1 shows, every level of the management structure will contain a mixture of both. At Level 1, Sargsyan (Comp Sci, member of *FastMath*) will be deploying advanced UQ tools to assess uncertainties in the properties calculated by Trelewicz, Szlufarska, Setyawan, and Cereceda by way of the interatomic potentials developed by Cusentino (Mat Sci). At Level 2, Marian and Humrickhouse (both Mat Sci) will be developing mesoscale models aided by Po (Mat/Comp Sci) and Bernholdt (Comp Sci). Lastly, Level 3 will involve work by Spencer (Mat/Comp Sci) and Permann (Comp Sci). As importantly, executive direction will be provided and shared by Marian (Mat Sci), Trelewicz (Mat Sci), and Bernholdt (Comp Sci).

4.3 Collaborations and connection to other FES/Scidac efforts

The present proposal concerns specific elements of the integrated fusion reactor structure, which makes it of interest to other fusion engineering and design efforts. We will work with other funded FES/SciDAC centers focused on plasma-materials interactions to define appropriate boundary conditions for our component-level simulations (Level 3). These will include helium and hydrogen isotope fluxes originating from the plasma edge, loss of thermal conductivity due to amorphization and/or fuss formation in the outermost layer of the W armor plates, and buildup of damage energy for grain growth and recrystallization simulations. Several ThermChem-FW team members, as of the application submission deadline, are part of the PSI2 project [150] (which is also responding to this FOA as "PMI-SciDAC") and will ensure a seamless coordination with our project. Joint participation by members of our team in this and other DOE-relevant programs are listed next:

SciDAC-5 Institutes	*FastMath*: Frameworks, Algorithms, and Scalable *Technologies* for Mathematics	Sargsyan (SNL)	[151]
FES/SciDAC Projects	*PSI2*: Predicting the Performance and Impact of Dynamic PFC Surfaces	Marian (UCLA), Cusentino (SNL), Setyawan (PNNL), Bernholdt (ORNL)	[152]
	AToM: Advanced Tokamak Modeling Environment	Bernholdt (ORNL)	[153]
NE/SciDAC Projects	Simulation of Fission Gas in Uranium Oxide Nuclear Fuel [1]	Permann (INL), Bernholdt (ORNL)	[154]
Other DOE-funded advanced simulation efforts	*NEAMS*: Nuclear Energy Advanced Modeling and Simulation	Permann (INL), Spencer (INL)	[155]

As well, a collaboration with ORNL's base fusion materials program led by Dr Yutai Katoh will be established to take advantage of the Japan-US collaboration to update the material properties handbook for F82H RAFM, particularly heavy-ion irradiation data up to 80 dpa [156]. Building on

[1] This project officially ended in FY22 but it continues to support a number of final activities with carryover funds.

this, we will interface with the "*Advance Castable Nanostructured Alloys for First Wall/Blanket Applications"* project [157], which focuses on building engineering databases for certain types of castable nanostructured alloys (CNA) [158] under the umbrella of the GAMOW effort [159]. These CNA are being developed as a new class of RAFM steels based on carbide-strengthened nanostructured alloys with the intent to demonstrate the viability of industry-scale CNA production. The scope of the collaboration will be to use CNA property data in our models for what we envision to potentially become the US reference RAFM steel for first wall and blanket components. The project is led by Dr Ying Yang at ORNL. A joint collaboration letter from ORNL program leader Katoh is attached to Appendix 6 at the end of this proposal.

Finally, the methods and models developed in this proposal will also be of interest to private fusion industry stakeholders to test and evaluate the performance of their FPP concepts under realistic operational scenarios. Here, we will partner with *Commonwealth Fusion Systems* (CFS) to deploy our integrated thermomechanical evolution prediction tools to their FPP design 'SPARC' [160]. A collaboration letter from CFS' Fusion Materials Lead Dr Cody Dennett is also attached to Appendix 6 at the end of the proposal.

4.4 Timeline of milestones and deliverables

A Gantt chart with the milestones and deliverables of the project is shown below. Milestones and deliverables are labeled as 'L[X]-M[Y]', where [X] refers to the Level they pertain to (1, 2 or 3) and [Y] is the internal task counter within each level. The main institutions involved in each task are highlighted in bold letters at the end of each bullet.

- L1-M1. Creation of the neutronics model of the reference component geometry using MCNP6.2 and DAGMC → (***ORNL***).
- L1-M2. Calculation of nuclide sequences for the three candidate materials under the expected conditions of FNSF → (***Villanova***).
- L1-M3. Development of ML-IAP for first wall components focused on capturing chemical composition changes due to transmutation → (***SNL***).
- L1-M4. Estimation and propagation of uncertainties in the development and use of ML-IAP → (***SNL***).
- L1-M5. Calculation of PKA energy distributions as a function of burnup using SPECTRA-PKA → (***Villanova, UCLA***).
- L1-M6. Calculation of irradiation defect cluster diffusivity using DFT, ML-IAP, and lattice kMC in all materials of interest → (***PNNL, UW, Stony Brook)***.
- L1-M7. Calculation of binding energies of irradiation defect clusters to selected transmutants using DFT and ML-IAP in all materials of interest → (***UW, Stony Brook, PNNL,***).
- L1-M8. Calculation of binding energies of He, vacancies, and transmutation products to the He-V clusters →(***PNNL, Stony Brook***).
- L1-M9. Calculation of the thermal conductivities and elastic constants as a function of evolving chemistry due to transmutation in all three materials of interest using the coupled DFT, MD, and BTE approach → (***UW, Stony Brook, Villanova***).
- L1-M10. Calculation of GB defect absorption efficiencies as a function of evolving chemistry due to transmutation using MD simulations based on MKL-IAP → (***Stony Brook ,UW***).
- L1-M11. Determination of tritium absorption/dissociation coefficients in FW-B interfaces→ (***Stony Brook, ORNL***).

- L2-M1. Adaptation of SCD code to large scale unstructured meshes via parallel synchronization approach → (***UCLA, Miami***).
- L2-M2. Development of the machine learning-assisted evolution model for defect size predictions in W, Fe-Cr, and SiC → (***PNNL, UCLA***).

L2-M3. Integrate machine learning evolution module with SCD code for irradiation damage module acceleration → (***PNNL, UCLA***).

L2-M4. Development of hardening/creep model using PX-CP framework, benchmarked to available experimental data → (***Miami***).

L2-M5. Extension of GG-RX model to capture irradiation defect accumulation driving force → (***UCLA***)

L2-M6. Simulations of grain growth under irradiation and estimation of critical RX temperatures → (***UCLA***).

L2-M7. Development of tritium transport/retention model → (***ORNL***).

L3-M1. Demonstrate use of GPU acceleration for evaluating neural network-based reduced order models within MOOSE → (***INL***).

L3-M2. Demonstrate use of web-interface-based capability for interacting with an external code that provides a high-fidelity model to compute quantities relevant for component-scale simulations → (***INL, Miami, ORNL***).

L3-M3. Demonstrate system for continuous online updating to improve fidelity of reduced order models → (***INL, Miami***).

L3-M4. Demonstrate component-level simulations of first wall/blanket and divertor structures using mesoscale-informed constitutive models → (***INL, ORNL, Miami, UCLA***).

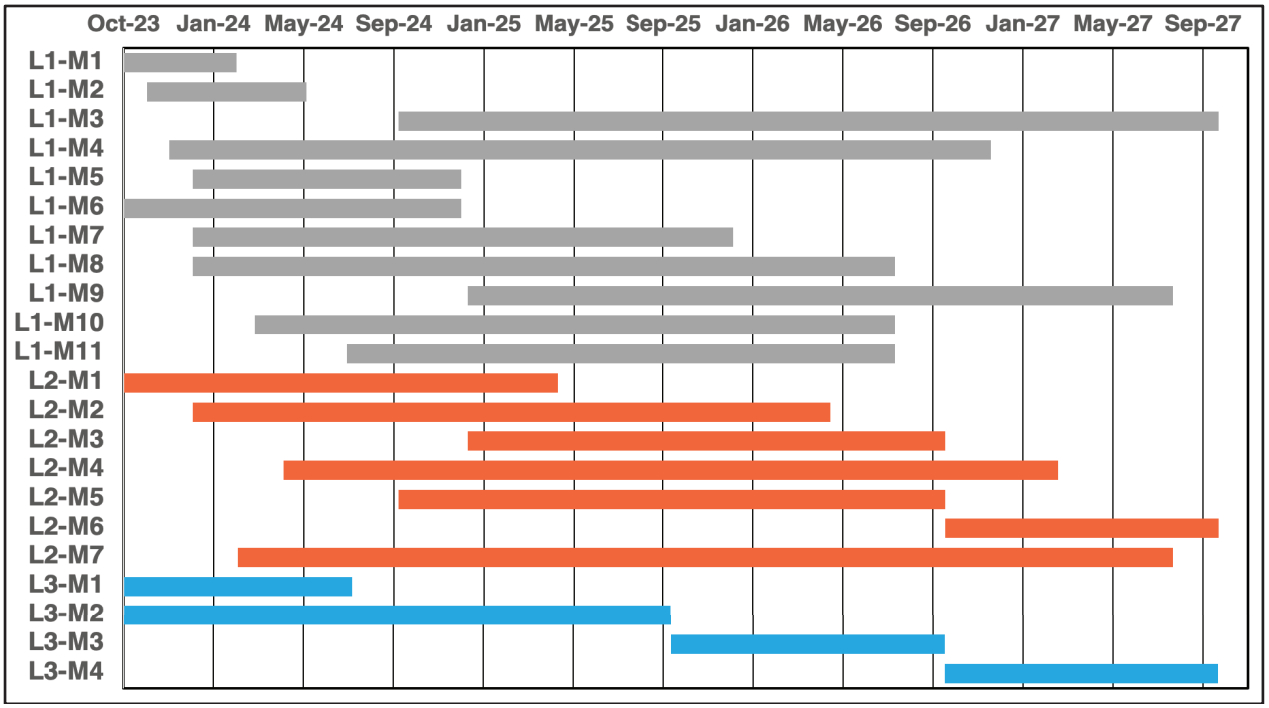

Appendix 1. Bibliography and references cited

1. M. S. Tillack, A. R. Raffray, X. R. Wang, S. Malang, S. Abdel-Khalik, M. Yoda, and D. Youchison. "Recent US activities on advanced He-cooled W-alloy divertor concepts for fusion power plants." *Fusion Engineering and Design* **86** (2011) 71-98.
2. J. Reiser, and M. Rieth. "Optimization and limitations of known DEMO divertor concepts." *Fusion Engineering and Design* **87** (2012) 718-721.
3. Y. Igitkhanov, B. Bazylev, and I. Landman. "CFC and W monoblock first wall concepts for fusion reactor." *Fusion Science and Technology* **62** (2012) 34-38.
4. Mohamed Abdou, Neil B. Morley, Sergey Smolentsev, Alice Ying, Siegfried Malang, Arthur Rowcliffe, Mike Ulrickson,"Blanket/first wall challenges and required R&D on the pathway to DEMO". *Fusion Engineering and Design* **100** (2015) 2-43.
5. L. El-Guebaly, A. Rowcliffe, J. Menard, and T. Brown. "TBM/MTM for HTS-FNSF: An Innovative Testing Strategy to Qualify/Validate Fusion Technologies for U.S. DEMO". *Energies* **9** (2016) 632.
6. Jochen Linke, Juan Du, Thorsten Loewenhoff, Gerald Pintsuk, Benjamin Spilker, Isabel Steudel, and Marius Wirtz. "Challenges for plasma-facing components in nuclear fusion." *Matter and Radiation at Extremes* **4** (2019) 056201.
7. R. Kembleton, M. Siccinio, F. Maviglia, and F. Militello. "Benefits and challenges of advanced divertor configurations in DEMO." *Fusion Engineering and Design* **179** (2022) 113120.
8. T. Ihli, T. K. Basu, L. M. Giancarli, S. Konishi, S. Malang, F. Najmabadi, S. Nishio et al. "Review of blanket designs for advanced fusion reactors." *Fusion Engineering and Design* **83** (2008) 912-919.
9. Rieth, M., Sergei L. Dudarev, SM Gonzalez De Vicente, J. Aktaa, T. Ahlgren, S. Antusch, D. E. J. Armstrong et al. "Recent progress in research on tungsten materials for nuclear fusion applications in Europe." *Journal of Nuclear Materials* **432** (2013) 482-500.
10. P. Norajitra. Divertor development for a future fusion power plant. **Vol. 1**. *KIT scientific publishing*, 2014.
11. D. Stork, Pietro Agostini, Jean-Louis Boutard, Derek Buckthorpe, Eberhard Diegele, Sergei L. Dudarev, Colin English et al. "Materials R&D for a timely DEMO: Key findings and recommendations of the EU Roadmap Materials Assessment Group." *Fusion engineering and design* **89** (2014) 1586-1594.
12. H. Hashizume, K. Miya, M. Seki, and K. Ioki. "Thermomechanical behavior of the first wall subjected to plasma disruption." *Fusion engineering and design* **5** (1987) 141-154.
13. R. Mattas, "Lifetime analysis of fusion reactor components." *Nuclear Technology-Fusion* **4** (1983) 1257-1262.
14. P. Chiovaro, P. Alessandro Di Maio, R. Giammusso, Q. Lupo, and G. Vella. "Thermal–mechanical and thermal–hydraulic integrated study of the Helium-Cooled

Lithium Lead Test Blanket Module." *Fusion engineering and design* **85** (2010) 1147-1153.

15. M. R. Gilbert, S. L. Dudarev, S. Zheng, L. W. Packer, and J-Ch Sublet. "An integrated model for materials in a fusion power plant: transmutation, gas production, and helium embrittlement under neutron irradiation." *Nuclear Fusion* **52** (2012) 083019.
16. Arunodaya Bhattacharya, Steven Zinkle, Jean Henry, Samara M. Levine, Philip D. Edmondson, Mark R. Gilbert, Hiroyasu Tanigawa, and Charles E. Kessel. "Irradiation damage concurrent challenges with RAFM and ODS steels for fusion reactor first-wall/blanket: a review." *Journal of Physics: Energy* **4** (2022) 034003.
17. Y. Huang, M. S. Tillack, N. M. Ghoniem, J. P. Blanchard, L. A. El-Guebaly, and C. E. Kessel. "Multiphysics modeling of the FW/Blanket of the US fusion nuclear science facility (FNSF)." *Fusion Engineering and Design* **135** (2018) 279-289.
18. H. Gwon, H. Tanigawa, T. Hirose, and Y. Kawamura. "Thermal mechanical characteristics of blanket first walls with different cooling channel shapes." *Fusion Engineering and Design* **136** (2018) 146-150.
19. P. Zacha, and S. Entler. "High heat flux limits of the fusion reactor water-cooled first wall." *Nuclear Engineering and Technology* **51** (2019) 1251-1260.
20. S. J. Zinkle, and N. M. Ghoniem. "Operating temperature windows for fusion reactor structural materials." *Fusion Engineering and design* **51** (2000) 55-71.
21. S. J. Zinkle, and L. L. Snead. "Designing radiation resistance in materials for fusion energy." *Annual Review of Materials Research* **44** (2014) 241-267.
22. Takanori Hirose, Takashi Nozawa, Roger E. Stoller, Dai Hamaguchi, Hideo Sakasegawa, Hiroyasu Tanigawa, Hisashi Tanigawa, Mikio Enoeda, Yutai Katoh, and Lance Lewis Snead. "Physical properties of F82H for fusion blanket design." *Fusion Engineering and Design* **89** (2014) 1595-1599.
23. A. Davis, M. Harb, L. El-Guebaly, P. Wilson, and E. Marriott. "Neutronics Aspects of the FESS-FNSF." *Fusion Engineering and Design* **135** (2018) 271-278.
24. F. B. Brown, M. E. Rising, and J. L. Alwin. *What's New with MCNP6. 2 and Whisper-1.1*. LA-UR-17-27992, 2017.
25. Paul Wilson, Timothy J. Tautges, Jason A. Kraftcheck, Brandon M. Smith, and Douglass L. Henderson. "Acceleration techniques for the direct use of CAD-based geometry in fusion neutronics analysis." *Fusion Engineering and Design* **85** (2010) 1759-1765.
26. J. C. Sublet, J. W. Eastwood, J. G. Morgan, M. R. Gilbert, M. Fleming, W. Arter. "FISPACT-II: An Advanced Simulation System for Activation, Transmutation and Material Modelling." *Nucl Data Sheets*. 2017 Jan 1; **139**: 77–137
27. M. Fleming, T. Stainer, M. R. Gilbert. "The FISPACT-II User Manual". 2018.
28. M. R. Gilbert, and J-Ch. Sublet. "PKA distributions: Contributions from transmutation products and from radioactive decay." *Nuclear Materials and Energy* **9** (2016) 576-580.
29. El-Guebaly, Laila A., Wahyu Setyawan, Charles H. Henager Jr, Richard J. Kurtz, and G. Robert Odette. "Neutron activation and radiation damage assessment for W-Ni-Fe

tungsten heavy alloys with variable Ni content." *Nuclear Materials and Energy* **29** (2021) 101092.

30. M. E. Sawan, Yutai Katoh, and Lance Lewis Snead. "Transmutation of silicon carbide in a fusion nuclear environment." *Journal of Nuclear Materials* **442** (2013) S370-S375.
31. Gergely Papp, Michael Drevlak, Tünde Fülöp, and Per Helander. "Runaway electron drift orbits in magnetostatic perturbed fields." *Nuclear Fusion* **51** (2011) 043004.
32. TENDL-2019 nuclear data library. Available from: https://tendl.web.psi.ch/tendl_2019/tendl2019.html
33. M. R. Gilbert, L. W. Packer, J-Ch. Sublet, R. A. Forrest. “Inventory simulations under neutron irradiation: Visualization techniques as an aid to materials design.” *Nucl Sci Eng*. **177** (2014) 291–306.
34. Y. Qian Y, M. R. Gilbert, L. Dezerald, D. Cereceda. “Using first-principles calculations to predict the mechanical properties of transmuting tungsten under first wall fusion power-plant conditions.” *J. Phys. Condens. Matter.* **33** (2021) 345901.
35. M. R. Gilbert, J. Marian, J-Ch. Sublet. “Energy spectra of primary knock-on atoms under neutron irradiation”. *Journal of Nuclear Materials* **467** (2015) 121–34.
36. M. R. Gilbert, and J-Ch. Sublet. "Differential dpa calculations with SPECTRA-PKA." *Journal of Nuclear Materials* **504** (2018) 101-108.
37. A. Bartok and R. C. G. Kondor, “On Representing Chemical Environments,” *Physical Review B* **87** (2013) 184115.
38. J. Behler and M. Parrinello, “Generalized Neural-Network Representation of High-Dimensional Potential-Energy Surfaces,” *Physical Review Letters* **98** (2007) 146401.
39. A. Shapeev, “Moment Tensor Potentials: A Systematically Improvable Interatomic Potentials,” *Multiscale Modeling and Simulation* **14** (2016) 1153–1173.
40. A. Thompson, L. Swiler, C. Trott, S. Foiles and G. Tucker, “Spectral Neighbor Analysis Method for Automated Generation of Quantum-Accurate Interatomic Potentials,” *Journal of Computational Physics* **285** (2015) 316–330.
41. Y. Zuo, C. Chen, X. Li, Z. Deng, Y. Chen, J. Behler, G. Csanyi, A. Shapeev, A. Thompson, M. Wood and S. Ong, “Performance and Cost Assessment of Machine Learning Interatomic Potentials,” *Journal of Physical Chemistry A*, **124** (2020) 731–745
42. K. Nguyen-Cong, J. Willman, S. Moore, et al., “Billion atom molecular dynamics simulations of carbon at extreme conditions and experimental time and length scales,” *Proceedings of the International Conference for High Performance Computing, Networking, Storage and Analysis* **3** (2021) 1–12.
43. X.-G. Li, C. Chen, H. Zheng, et al., “Complex strengthening mechanisms in the NbMoTaW multi-principal element alloy," *npj Computational Materials* **6** (2020) 1–10.
44. S. Nikolov, M. Wood, A. Cangi, et al., “Data-driven magneto-elastic predictions with scalable classical spin-lattice dynamics,” *npj Computational Materials* **7** (2021) 1–12.

45. M. A. Wood, M. A. Cusentino, B. D. Wirth, et al., “Data-driven material models for atomistic simulation,” *Physical Review B* **99** (2019) 184305.
46. M. A. Cusentino, M. A. Wood, and A. P. Thompson, “Suppression of helium bubble nucleation in beryllium exposed tungsten surfaces,” *Nuclear Fusion* **60** (2020) 126018.
47. M. A. Cusentino, M. A. Wood, and A. P. Thompson, “Beryllium-driven structural evolution at the divertor surface,” *Nuclear Fusion* **61** (2021) 046049
48. A. Rohskopf, C. Sieviers, N. Lubbers, et al., “FitSNAP: Atomistic machine learning with LAMMPS,” *Journal of Open Source Software* **8** (2023) 5118
49. J.M. Goff, C. Sievers, M. A. Wood, and A. P. Thompson, “Permutation-adapted complete and independent basis for atomic cluster expansion descriptors,” arXiv:2208.01756, 2022.
50. J. Tranchida, S.J. Plimpton, P. Thibaudeau, and A.P. Thompson, “Massively parallel symplectic algorithm for coupled magnetic spoin dynamics and molecular dynamics”, *J. Comp. Phys.* **372** (2018) 406-425
51. A.P. Thompson, et al., “LAMMPS - a flexible simulation tool for particle-based materials modeling at the atomic, meso, and continuum scales”, *Comp Phys Comm*, **271** (2022) 10817.
52. S. Nikolov, M. Wood, A. Cangi, et al., “Data-driven magneto-elastic predictions with scalable classical spin-lattice dynamics,” *npj Computational Materials* **7** (2021) 1–12.
53. K. Sargsyan, X. Huan, and H. N. Najm, “Embedded Model Error Representation for Bayesian Model Calibration”, *Int J Uncert Quantif*, **9** (2019), 365-294
54. K. Sargsyan, “QUiNN: Quantification of Uncertainties in Neural Networks”, www.github.com/sandialabs/quinn
55. Sargsyan, “Surrogate Models for Uncertainty Propagation and Sensitivity Analysis.” In *Handbook of Uncertainty Quantification*, **Chapter 19** (2016). https://doi.org/10.1007/978-3-319-11259-6_22-1.
56. Wahyu Setyawan, Aaron P. Selby, Niklas Juslin, Roger E. Stoller, Brian D. Wirth, and Richard J. Kurtz. "Cascade morphology transition in bcc metals." *Journal of Physics: Condensed Matter* **27** (2015) 225402.
57. Wahyu Setyawan, Giridhar Nandipati, Kenneth J. Roche, Howard L. Heinisch, Brian D. Wirth, and Richard J. Kurtz. "Displacement cascades and defects annealing in tungsten, Part I: Defect database from molecular dynamics simulations." *Journal of Nuclear Materials* **462** (2015) 329-337.
58. A. De Backer, Christophe Domain, C. S. Becquart, L. Luneville, D. Simeone, Andrea E. Sand, and Kai Nordlund. "A model of defect cluster creation in fragmented cascades in metals based on morphological analysis." *Journal of Physics: Condensed Matter* **30** (2018) 405701.
59. Roger E. Stoller, and Eva Zarkadoula. "Primary radiation damage formation in solids." (2020) 620-662.

60. Andrea E. Sand, D. R. Mason, A. De Backer, X. Yi, S. L. Dudarev, and K. Nordlund. "Cascade fragmentation: deviation from power law in primary radiation damage." *Materials Research Letters* **5** (2017) 357-363.
61. Jun Fu, Yangchun Chen, Jingzhong Fang, Ning Gao, Wangyu Hu, Chao Jiang, Hong-Bo Zhou, Guang-Hong Lu, Fei Gao, and Huiqiu Deng. "Molecular dynamics simulations of high-energy radiation damage in W and W–Re alloys." *Journal of Nuclear Materials* **524** (2019) 9-20.
62. C. Liu, and I. Szlufarska. "Distribution of defect clusters in the primary damage of ion irradiated 3C-SiC." *Journal of nuclear materials* **509** (2018) 392-400.
63. Xinhua Yang, Ying Zheng, and Jie Li. "Evaluation of Cr Concentration Effect on Displacement Cascades in Fe–Cr Alloys with Piecewise Potential." *Acta Mechanica Solida Sinica* **33** (2020) 239-250.
64. Graeme Henkelman, and Hannes Jónsson. "Improved tangent estimate in the nudged elastic band method for finding minimum energy paths and saddle points." *The Journal of chemical physics* **113** (2000) 9978-9985.
65. Chen-Hsi Huang, Leili Gharaee, Yue Zhao, Paul Erhart, and Jaime Marian. "Mechanism of nucleation and incipient growth of Re clusters in irradiated W-Re alloys from kinetic Monte Carlo simulations." *Physical Review B* **96** (2017) 094108
66. Hao Jiang, Chao Jiang, Dane Morgan, and Izabela Szlufarska. "Accelerated atomistic simulation study on the stability and mobility of carbon tri-interstitial cluster in cubic SiC." *Computational materials science* **89** (2014) 182-188.
67. Charlotte S. Becquart, Christophe Domain, Utpal Sarkar, Andrée Debacker, and Marc Hou. "Microstructural evolution of irradiated tungsten: Ab initio parameterisation of an OKMC model." *Journal of nuclear materials* **403** (2010) 75-88.
68. Wahyu Setyawan, Giridhar Nandipati, and Richard J. Kurtz. "Ab initio study of interstitial cluster interaction with Re, Os, and Ta in W." *Journal of Nuclear Materials* **484** (2017) 30-41
69. Li-Peng Wang, Wen Yang, Zhang-Bo Ma, Jia-Hong Zhu, and Yong-Tang Li. "First-principles study of chromium diffusion in the ferritic Fe-Cr alloy." *Computational Materials Science* **181** (2020) 109733.
70. Pablo Bruzzoni, and Roberto Cesar Pasianot. "A DFT study of H solubility and diffusion in the Fe-Cr system." *Computational Materials Science* **154** (2018) 243-250.
71. Pär Olsson,"Ab initio study of interstitial migration in Fe–Cr alloys." *Journal of nuclear materials* **386** (2009) 86-89.
72. Shenyang Hu, Wahyu Setyawan, Renee M. Van Ginhoven, Weilin Jiang, Charles H. Henager Jr, and Richard J. Kurtz. "Thermodynamic and kinetic properties of intrinsic defects and Mg transmutants in 3C–SiC determined by density functional theory." *Journal of nuclear materials* **448** (2014) 121-128.

73. Wenyi Wang, Chuan Li, Shun-Li Shang, Jianzhu Cao, Zi-Kui Liu, Yi Wang, and Chao Fang. "Diffusion of hydrogen isotopes in 3C-SiC in HTR-PM: A first-principles study." *Progress in Nuclear Energy* **119** (2020) 103181.
74. Sun, Jingjing, Yu-Wei You, Jie Hou, Xiangyan Li, B. S. Li, C. S. Liu, and Z. G. Wang. "The effect of irradiation-induced point defects on energetics and kinetics of hydrogen in 3C-SiC in a fusion environment." *Nuclear Fusion* **57** (2017) 066031.
75. Chartier Alain, and Meis Constantin. "Theoretical study of helium insertion and diffusion in 3C-SiC." *Journal of Nuclear Materials* **348** (2006).
76. Danny Perez, Thomas Vogel, and Blas P. Uberuaga. "Diffusion and transformation kinetics of small helium clusters in bulk tungsten." *Physical Review B* **90** (2014) 014102.
77. H. Q. Deng, W. Y. Hu, Fei Gao, Howard L. Heinisch, Shenyang Y. Hu, Y. L. Li, and Richard J. Kurtz. "Diffusion of small He clusters in bulk and grain boundaries in α-Fe." *Journal of Nuclear Materials* **442** (2013) S667-S673.
78. M. Z. Hossain, and Jaime Marian. "Stress-dependent solute energetics in W-Re alloys from first-principles calculations." *Acta materialia* **80** (2014) 107-117.
79. Leili Gharaee, Jaime Marian, and Paul Erhart. "The role of interstitial binding in radiation induced segregation in W-Re alloys." *Journal of Applied Physics* **120** (2016) 025901.
80. Tomoaki Suzudo, Masatake Yamaguchi, and Akira Hasegawa. "Migration of rhenium and osmium interstitials in tungsten." *Journal of Nuclear Materials* **467** (2015) 418-423.
81. Alejandro Londono-Hurtado, Andrew J. Heim, Sungtae Kim, Izabela Szlufarska, and Dane Morgan. "Cs and Ag co-incorporation in cubic silicon carbide." *Journal of nuclear materials* **439** (2013) 65-71.
82. Amy Kaczmarowski, Shujiang Yang, Izabela Szlufarska, and Dane Morgan. "Genetic algorithm optimization of defect clusters in crystalline materials." *Computational Materials Science* **98** (2015) 234-244.
83. Krister OE Henriksson, Kai Nordlund, Arkady Krasheninnikov, and Juhani Keinonen. "The depths of hydrogen and helium bubbles in tungsten: a comparison." *Fusion science and technology* **50** (2006) 43-57.
84. M. Samaras. "Multiscale modelling: the role of helium in iron." *Materials Today* **12** (2009) 46-53.
85. G. Lucas, and R. Schäublin. "Stability of helium bubbles in alpha-iron: A molecular dynamics study." *Journal of nuclear materials* **386** (2009) 360-362.
86. Daniel Brimbal, Brigitte Décamps, Alain Barbu, Estelle Meslin, and Jean Henry. "Dual-beam irradiation of α-iron: Heterogeneous bubble formation on dislocation loops." *Journal of Nuclear Materials* **418** (2011) 313-315.
87. R. E. Stoller, and Yu N. Osetsky. "An atomistic assessment of helium behavior in iron." *Journal of Nuclear Materials* **455** (2014) 258-262.
88. M. Miyamoto, S. Mikami, H. Nagashima, N. Iijima, D. Nishijima, R. P. Doerner, N. Yoshida, Hideo Watanabe, Y. Ueda, and A. Sagara. "Systematic investigation of the

formation behavior of helium bubbles in tungsten." *Journal of Nuclear Materials* **463** (2015) 333-336.

89. Shi-Hao Li, Jing-Ting Li, and Wei-Zhong Han. "Radiation-induced helium bubbles in metals." *Materials* **12** (2019) 1036.
90. Iuliia Ipatova, Graeme Greaves, Salvador Pacheco-Gutiérrez, S. C. Middleburgh, M. J. D. Rushton, and Enrique Jimenez-Melero. "In-situ TEM investigation of nano-scale helium bubble evolution in tantalum-doped tungsten at 800° C." *Journal of Nuclear Materials* **550** (2021) 152910.
91. D. Perez, L. Sandoval, S. Blondel, S. *et al.* "The mobility of small vacancy/helium complexes in tungsten and its impact on retention in fusion-relevant conditions." *Sci. Rep.* **7** (2017) 2522.
92. A. Hasegawa, T. Tanno, S. Nogami, M. Satou. "Property change mechanism in tungsten under neutron irradiation in various reactors", *Journal of Nuclear Materials* **417** (2011) 491-494.
93. M. Akiyoshi, L.M. Garrison, J.W. Geringer, H. Wang, A. Hasegawa, S. Nogami, Y. Katoh. "Thermal diffusivity of irradiated tungsten and tungsten-rhenium alloys", *Journal of Nuclear Materials* **543** (2021) 152594.
94. S. X. Zhou, R. Jacobs, W. Xie, E. Tea, C. Hin, and D. Morgan, "Combined Ab Initio and Empirical Model of the Thermal Conductivity of Uranium, Uranium-Zirconium, and Uranium-Molybdenum", *Physical Review Materials* **2** (2018).
95. S. X. Zhou, R. Jacobs, Y. F. Zhang, C. Jiang, and D. Morgan, "Combined Ab-Initio and Empirical Model for Irradiated Metal Alloys with a Focus on Uranium Alloy Fuel Thermal Conductivity", *Journal of Nuclear Materials* **549** (2021).
96. S. X. Zhou, Y. F. Zhang, C. Jiang, and D. Morgan, A Combined Ab-Initio and Empirical Model for Thermal Conductivity of Concentrated Metal Alloys with the Focus on Binary Uranium Alloys, *Materialia* **15** (2021).
97. S. X. Zhou, Y. F. Zhang, and D. Morgan, An Ab-Initio Based Semi-Empirical Thermal Conductivity Model for Multiphase Uranium-Zirconium Alloys, *Journal of Nuclear Materials* **553** (2021).
98. J. M. Ziman, "Electrons and Phonons: The Theory of Transport Phenomena in Solids". (1960).
99. T. M. Tritt, Thermal Conductivity: Theory, Properties, and Applications. (2006)
100. B. Dongre, J. Carrete, S. Wen, J. Ma, W. Li, N. Mingo, and G. K. H. Madsen, Combined Treatment of Phonon Scattering by Electrons and Point Defects Explains the Thermal Conductivity Reduction in Highly-Doped Si, *Journal of Materials Chemistry A* **8** (2020) 1273-1278.
101. G. K. H. Madsen and D. J. Singh, "Boltztrap. A Code for Calculating Band-Structure Dependent Quantities", *Computer Physics Communications* **175** (2006) 67-71.
102. A. Togo, "First-Principles Phonon Calculations with Phonopy and Phono3py", *Journal of the Physical Society of Jap[an* **92** (2023).

103. A. Togo and I. Tanaka, “First Principles Phonon Calculations in Materials Science”, *Scripta Materialia* **108** (2015) 1-5.
104. Shuang Cui, Michael Simmonds, Wenjing Qin, Feng Ren, George R. Tynan, Russell P. Doerner, and Renkun Chen. "Thermal conductivity reduction of tungsten plasma facing material due to helium plasma irradiation in PISCES using the improved 3-omega method." *Journal of Nuclear Materials* **486** (2017) 267-273.
105. Felix Hofmann, Daniel R. Mason, Jeffrey K. Eliason, Alexei A. Maznev, Keith A. Nelson, and Sergei L. Dudarev. "Non-contact measurement of thermal diffusivity in ion-implanted nuclear materials." *Scientific reports* **5** (2015) 1-7.
106. Daniel R. Mason, Abdallah Reza, Fredric Granberg, and Felix Hofmann. "Estimate for thermal diffusivity in highly irradiated tungsten using molecular dynamics simulation." *Physical Review Materials* **5** (2021) 125407.
107. J. Marian, G. Venturini, B. L. Hansen, J. Knap, M. Ortiz, and G. H. Campbell. "Finite-temperature extension of the quasicontinuum method using langevin dynamics: entropy losses and analysis of errors." *Modelling and Simulation in Materials Science and Engineering* **18** (2009) 015003.
108. X. Hu, C.M. Parish, K. Wang, T. Koyanagi, B.P. Eftink, Y. Katoh. “Transmutation-induced precipitation in tungsten irradiated with a mixed energy neutron spectrum”, *Acta Materialia* **165** (2019) 51-61.
109. R. G. Faulkner, Shenhua Song, P. E. J. Flewitt, M. Victoria, and P. Marmy. "Grain boundary segregation under neutron irradiation in dilute alloys." *Journal of nuclear materials* **255** (1998) 189-209.
110. Bo Zhang, Yu-Hao Li, Hong-Bo Zhou, Huiqiu Deng, and Guang-Hong Lu. "Segregation and aggregation of rhenium in tungsten grain boundary: Energetics, configurations and strengthening effects." *Journal of Nuclear Materials* **528** (2020) 151867.
111. A.G. Froseth, H. Van Swygenhoven, P.M. Derlet. “Developing realistic grain boundary networks for use in molecular dynamics simulations”, *Acta Materialia* **53** (2005) 4847-4856.
112. B. Sadigh, P. Erhart, A. Stukowski, A. Caro, E. Martinez, L. Zepeda-Ruiz. “Scalable parallel Monte Carlo algorithm for atomistic simulations of precipitation in alloys”, *Physical Review B* **85** (2012)
113. Juo Chai, Shuo Jin, Ziang Yu, Haixuan Xu, and Guang-Hong Lu. "Capture efficiency and bias from the defect dynamics near grain boundaries in BCC Fe using mesoscale simulations." *Journal of Materials Science & Technology* **93** (2021) 169-177.
114. Yejun Gu, Jian Han, Shuyang Dai, Yichao Zhu, Yang Xiang, and David J. Srolovitz. "Point defect sink efficiency of low-angle tilt grain boundaries." *Journal of the Mechanics and Physics of Solids* **101** (2017) 166-179.
115. Yongfeng Zhang, Hanchen Huang, Paul C. Millett, Michael Tonks, Dieter Wolf, and Simon R. Phillpot. "Atomistic study of grain boundary sink strength under prolonged electron irradiation." *Journal of Nuclear Materials* **422** (2012) 69-76.

116. Blas Pedro Uberuaga, Louis J. Vernon, Enrique Martinez, and Arthur F. Voter. "The relationship between grain boundary structure, defect mobility and grain boundary sink efficiency." *Scientific reports* **5** (2015) 9095.
117. S. J. Zinkle, and N. M. Ghoniem. "Operating temperature windows for fusion reactor structural materials." *Fusion Engineering and design* **51** (2000) 55-71.
118. Arunodaya Bhattacharya, Steven Zinkle, Jean Henry, Samara M. Levine, Philip D. Edmondson, Mark R. Gilbert, Hiroyasu Tanigawa, and Charles E. Kessel. "Irradiation damage concurrent challenges with RAFM and ODS steels for fusion reactor first-wall/blanket: a review." *Journal of Physics: Energy* (2022).
119. Z. X. Zhang, D. S. Chen, W. T. Han, and A. Kimura. "Irradiation hardening in pure tungsten before and after recrystallization." *Fusion Engineering and Design* **98** (2015) 2103-2107.
120. V. Shah, J. A. W. van Dommelen, E. Altstadt, A. Das, and M. G. D. Geers. "Brittle-ductile transition temperature of recrystallized tungsten following exposure to fusion relevant cyclic high heat load." *Journal of Nuclear Materials* **541** (2020) 152416.
121. H. Ma, Alla S. Sologubenko, Max Döbeli, Kay Sanvito, Alex Heusi, Kaj Pletscher, and Ralph Spolenak. "The curious mechanism of irradiation-induced cryogenic grain growth in tungsten thin films: a pathway to single crystals." *Acta Materialia* **187** (2020) 153-165.
122. V. Shah, M. P. F. H. L. van Maris, J. A. W. van Dommelen, and M. G. D. Geers. "Experimental investigation of the microstructural changes of tungsten monoblocks exposed to pulsed high heat loads." *Nuclear Materials and Energy* **22** (2020) 100716.
123. S. Nogami, Dmitry Terentyev, Aleksandr Zinovev, Chao Yin, Michael Rieth, Gerald Pintsuk, and Akira Hasegawa. "Neutron irradiation tolerance of potassium-doped and rhenium-alloyed tungsten." *Journal of Nuclear Materials* **553** (2021) 153009.
124. W. S. Cunningham, Khalid Hattar, Yuanyuan Zhu, Danny J. Edwards, and Jason R. Trelewicz. "Suppressing irradiation induced grain growth and defect accumulation in nanocrystalline tungsten through grain boundary doping." *Acta Materialia* **206** (2021) 116629.
125. H. Gietl, Takaaki Koyanagi, Xunxiang Hu, Makoto Fukuda, Akira Hasegawa, and Yutai Katoh. "Neutron irradiation-enhanced grain growth in tungsten and tungsten alloys." *Journal of Alloys and Compounds* **901** (2022) 163419
126. P. Schuster, "Taming combinatorial explosion." *Proceedings of the National Academy of Sciences* **97** (2000) 7678-7680.
127. J. Marian, and Vasily V. Bulatov. "Stochastic cluster dynamics method for simulations of multispecies irradiation damage accumulation." *Journal of Nuclear Materials* **415** (2011) 84-95.
128. S. Schmitt, "Sparse matrices in numerical methods for differential equations," *Acta Numerica* **19** (2010) 403-534.
129. E. Hairer, S. P. Nørsett, and G. Wanner, Solving Ordinary Differential Equations I: Nonstiff Problems, 2nd ed. Berlin: Springer, 1993.

130. Qianran Yu, Michael J. Simmonds, Russ Doerner, George R. Tynan, Li Yang, Brian D. Wirth, and Jaime Marian. "Understanding hydrogen retention in damaged tungsten using experimentally-guided models of complex multispecies evolution." *Nuclear Fusion* **60** (2020) 096003.
131. Chen-Hsi Huang, Mark R. Gilbert, and Jaime Marian. "Simulating irradiation hardening in tungsten under fast neutron irradiation including Re production by transmutation." *Journal of Nuclear Materials* **499** (2018) 204-215.
132. D. T. Gillespie, "Monte Carlo simulation of random walks with residence time dependent transition probability rates." *Journal of Computational Physics* **28** (1978): 395-407.
133. Yucheng Fu, William E. Frazier, Kyoo Sil Choi, Lei Li, Zhijie Xu, Vineet V. Joshi, and Ayoub Soulami. "Prediction of grain structure after thermomechanical processing of U-10Mo alloy using sensitivity analysis and machine learning surrogate model." *Scientific Reports* **12** (2022) 10917.
134. Shao-Ching Huang and John Kim, The Effects Of Interface Deformation Of Superhydrophobic Surface On Wall Turbulence, 16th European Turbulence Conference, 21-24 August, 2017, Stockholm, Sweden, 2017.
135. Shao-Ching Huang, An immersed boundary method with mesh refinement for turbulent flow simulations, 72nd Annual Meeting of the APS Division of Fluid Dynamics, 2019.
136. Qianran Yu, Giacomo Po, and Jaime Marian. "Physics-based model of irradiation creep for ferritic materials under fusion energy operation conditions." *Journal of Applied Physics* **132** (2022) 225101.
137. Anirban Patra, and David L. McDowell. "Crystal plasticity-based constitutive modelling of irradiated bcc structures." *Philosophical Magazine* **92** (2012) 861-887.
138. Q. Yu, Qianran, S. Chatterjee, K. J. Roche, G. Po, and J. Marian. "Coupling crystal plasticity and stochastic cluster dynamics models of irradiation damage in tungsten." *Modelling and Simulation in Materials Science and Engineering* **29** (2021) 055021.
139. Xiazi Xiao, Dmitry Terentyev, Long Yu, A. Bakaev, Zhaohui Jin, and Huiling Duan. "Investigation of the thermo-mechanical behavior of neutron-irradiated Fe-Cr alloys by self-consistent plasticity theory." *Journal of Nuclear Materials* **477** (2016) 123-133.
140. D. Terentyev, C.-C. Chang, C. Yin, A. Zinovev and X.-F He. “Neutron irradiation effects on mechanical properties of ITER specification tungsten”, *Tungsten* **3** (2021) 415-433.
141. D. Brunner. “Comparison of flow-stress measurements on high-purity tungsten single crystals with the kink-pair theory”. *Materials Transactions*, JIM **41**(2000) 152-160.
142. A.S. Argon and S.R. Maloof. “Plastic deformation of tungsten single crystals at low temperatures.” *Acta metallurgica*, **14** (1966) 1449-1462.
143. H. Schultz. “Defect-sensitive properties of tungsten and other bcc transition metals.” *Z. Metallkd* **78** (1987).
144. C. McElfresh, and J. Marian. "Initial grain orientation controls static recrystallization outcomes in cold-worked iron: Insight from coupled crystal plasticity/vertex dynamics modeling." *Acta Materialia* **245** (2023) 118631.

145. A. Mannheim, J. A. W. Van Dommelen, and M. G. D. Geers. "Modelling recrystallization and grain growth of tungsten induced by neutron displacement defects." *Mechanics of Materials* **123** (2018) 43-58.
146. G. R. Longhurst, "TMAP7 User Manual," INEEL/EXT-04-02352, 2004.
147. A. D. Lindsay, et al. “2.0-MOOSE: Enabling massively parallel multiphysics simulation”. *SoftwareX*. **20** (2022) 101202
148. A. E. Slaughter, Z. M. Prince, P. German, I. Halvic, W. Jiang, B. W. Spencer, S. L. Dhulipala, D. R. Gaston, “MOOSE Stochastic Tools: A module for performing parallel, memory-efficient in situ stochastic simulations”. *SoftwareX*. **22** (2023) 101345.
149. P. German, D. Yushu. “Enabling Scientific Machine Learning in MOOSE Using Libtorch”. Available at SSRN 4374315.
150. https://www.scidac.gov/institutes.html
151. https://www.scidac.gov/institutes.html
152. https://confluence.cels.anl.gov/display/PSIscidac2
153. https://atom.scidac.io
154. https://confluence.cels.anl.gov/display/FissionGasSciDAC2
155. https://neams.inl.gov
156. T. Nozawa, H. Tanigawa, T. Kojima, T. Itoh, N. Hiyoshi, M. Ohata, T. Kato, M. Ando, M. Nakajima, T. Hirose, J. D. Reed, X. Chen, J. W. Geringer, and Y. Katoh, "The status of the Japanese material properties handbook and the challenge to facilitate structural design criteria for DEMO in-vessel components", *Nucl. Fusion* **61** (2021) 116054.
157. https://arpa-e.energy.gov/technologies/projects/advance-castable-nanostructured-alloys-first-wallblanket-applications
158. L. Tan, Y. Katoh, L.L. Snead, "Development of castable nanostructured alloys as a new generation RAFM steels", *Journal of Nuclear Materials* **511** (2018) 598-604.
159. https://arpa-e.energy.gov/technologies/programs/gamow
160. https://cfs.energy/technology/sparc